Increased presynaptic excitability in a migraine with aura mutation

Pratyush Suryavanshi[1,2,3], Punam Sawant-Pokam[1], Sarah Clair[1], KC Brennan[1]

Abstract

Migraine is a common and disabling neurological disorder. The headache and sensory amplifications that characterize migraine are attributed to hyperexcitable sensory circuits, but a detailed understanding remains elusive. This is partly due to the paucity of genetic animal models associated with the common, less severe form of the disease. A mutation in casein kinase 1 delta (CK1δ) was identified in familial migraine with aura and advanced sleep phase syndrome. Spreading depolarization (SD), the phenomenon that underlies migraine aura, is facilitated in mice carrying one of the mutations ($CK1\delta_{T44A}$). However, the mechanism of this susceptibility is not known. We used a combination of whole-cell electrophysiology and imaging, *in vivo* and in *ex vivo* brain slices, to understand the cellular and synaptic underpinnings of this apparent circuit excitability. We found that despite normal synaptic activity and hyperpolarized neuronal membrane potentials at rest, $CK1\delta_{T44A}$ neurons were more excitable upon repetitive stimulation compared to wild-type (WT) controls. This was due to reduced presynaptic adaptation to high-frequency stimuli at excitatory, but not inhibitory synapses. Reduced adaptation at glutamatergic $CK1\delta_{T44A}$ synapses was mediated by a calcium-dependent enhancement of the size of the readily releasable pool of synaptic vesicles. This caused an increase in the cumulative amplitude of excitatory currents, and a higher excitation-to-inhibition ratio during sustained activity, both *in vivo* and in brain slices. Fluorescence imaging revealed increased glutamate release in $CK1\delta_{T44A}$ compared to WT brain slices, corroborating the presynaptic gain of function observed with electrophysiology. Action potential bursts elicited in individual $CK1\delta_{T44A}$ neurons enhanced glutamatergic feedback excitation within local microcircuits, further amplifying firing frequencies. At a network level *in vivo*, $CK1\delta_{T44A}$ mice showed increased duration of up state activity, which is dependent on recurrent excitation. Finally, we demonstrated that SD susceptibility of $CK1\delta_{T44A}$ brain slices could be returned to WT levels with the same reductions in extracellular calcium that normalized presynaptic adaptation. Taken together, these findings show a stimulus-dependent presynaptic gain of function at glutamatergic synapses in a genetic model of migraine, that accounts for the increased SD susceptibility and may also explain the sensory amplifications that are associated with the disease.

Author affiliations:

1 Department of Neurology, University of Utah School of Medicine, Salt Lake City, UT, USA

2 Interdepartmental Neuroscience Program, University of Utah School of Medicine, Salt Lake City, UT, USA

3 Department of Pediatrics, University of Iowa, Iowa City, IA, USA

Correspondence to: KC Brennan

Full address: 729 Arapeen Dr #1300, Salt Lake City, UT 84108

E-mail: k.c.brennan@hsc.utah.edu

Running title: Hyperexcitability in the casein kinase 1 delta mutant ($CK1\delta_{T44A}$) mouse

Keywords: Non-hemiplegic migraine with aura; presynaptic vesicle priming; sensory habituation, excitation-inhibition imbalance, monogenic migraine models.

Abbreviations: CK1δ: casein kinase-1δ; FHM: familial hemiplegic migraine; SD: spreading depolarization; S1 L2/3: primary somatosensory cortical layer 2/3; RRP: readily releasable pool; E/IPSCs: excitatory/inhibitory postsynaptic currents.

Introduction

Migraine affects about 12% of the world population and causes enormous disability, especially to women and to those in working and childbearing years.[1,2] Yet the disease remains poorly understood at the cellular and circuit level. Although migraine is typically associated with headaches, multiple lines of evidence suggest it is better characterized as a disorder of multi-sensory gain.[3] In addition to the headache, migraine attacks involve amplification of sensory percepts including light, sound, smell, touch, and enteroception (allodynia, photophobia, phonophobia, osmophobia, and nausea, respectively).[4,5] Migraine sufferers also exhibit larger amplitude sensory-evoked responses, and reduced habituation to repeated sensory stimulation during attacks and inter-ictal periods.[6–8] In a third of migraineurs, the attack is preceded by an aura, which is caused by a massive spreading depolarization (SD) of cortical tissue.[3,9]

The mechanisms underlying the aberrant sensory network activity in migraine are poorly understood. Animal models of monogenic forms of migraine offer unique mechanistic insight,[10] as mutations in single genes, and resultant dysregulation of downstream molecular

pathways, produce migraine phenotypes. Established monogenic mouse models harbor mutations found in familial hemiplegic migraine (FHM types 1 and 2) and exhibit an increased probability of release and impaired clearance at glutamatergic synapses, respectively.[11–14] These convergent lines of evidence suggest that increased synaptic excitability is a potential unifying mechanism of the disease. However, these models represent rare and severe forms of migraine, in which the migraine attacks are accompanied by hemiplegia.[11] It is thus of interest to determine whether such mechanisms apply more broadly.

Loss of function mutations in casein kinase 1 delta (CK1δ) were recently identified in two families exhibiting familial migraine with aura and advanced sleep phase syndrome.[15] Unlike FHM mutations, the CK1δ mutations segregate with phenotypically common migraine with aura. Mice carrying one of the mutations ($CK1\delta_{T44A}$) exhibit increased sensitivity to tactile and thermal hyperalgesia elicited by the migraine trigger nitroglycerin (NTG), as well as increased susceptibility to SD,[15] thus confirming that two key phenotypes of the disease are represented in the animal model. However, the $CK1\delta_{T44A}$ mutation affects a ubiquitous serine-threonine kinase with broad roles regulating normal cellular function.[16–19] Thus, although the molecular moiety responsible for the migraine phenotypes in $CK1\delta_{T44A}$ mice is known, the underlying cellular and synaptic mechanisms remain elusive. Here, using whole-cell electrophysiology and imaging *in vivo* and in brain slices, we uncovered presynaptic mechanisms contributing to SD susceptibility in $CK1\delta_{T44A}$ mice.

Materials and methods

Animal handling and experimental design

All experiments were conducted in accordance with and approved by the Institutional Animal Care and Use Committee at the University of Utah. Experiments were conducted on 2 – 3-month-old male $CK1\delta_{T44A}$ and wild-type (WT) littermate mice (line 827)[15,20] weighing between 20 and 30 g. Animals were housed in temperature-controlled rooms on a 12-hour light-dark cycle. The sample size was determined using data from preliminary experiments as well as previous reports, generally n=5-9 mice for *in vivo* and n=15-20 slices (7-10 mice) for *in vitro* experiments. For patch-clamp electrophysiology, recordings were obtained from 1 neuron per mouse (*in vivo*) or 1-2 neurons per slice (*in vitro*). Experimenters were blind to the animal genotypes in all experiments. Most comparisons were made across genotypes within the same condition or across conditions within the same animal or slice (paired or repeated measures).

In vitro brain slice preparation

$CK1\delta_{T44A}$ and WT littermate mice were deeply anesthetized with 4% isoflurane, and the brain was removed for slice preparation. Coronal sections were cut in ice-cold dissection buffer (in mM; 220 Sucrose, 3 KCl, 10 $MgSO_4$, 1.25 NaH_2PO_4, 25 $NaHCO_3$, 25 D-glucose, 1.3 $CaCl_2$), and sections containing somatosensory cortex[21] were allowed to recover in a chamber containing normal artificial cerebrospinal fluid (ACSF: in mM; 125 NaCl, 3 KCl, 1.3 $MgSO_4$, 1.25 NaH_2PO_4, 25 $NaHCO_3$, 25 D-glucose, 1.3 $CaCl_2$, and saturated with 95%O_2 / 5%CO_2) at 35°C. For electrophysiology experiments, the slices were transferred to a submerged chamber constantly supplied with ACSF (flow rate: 2.5 mL/min, saturated with 95%O_2 / 5%CO_2) also maintained at 35°C. In experiments manipulating extracellular calcium concentrations ($[Ca^{2+}]_e$), ACSF containing 0.65 mM $CaCl_2$ and 1.95mM $MgCl_2$ was used *after* slice incubation.

In vitro whole-cell electrophysiology

All whole-cell patch-clamp recordings were obtained from regular spiking pyramidal neurons[21] in layer 2/3 (L2/3) somatosensory cortex visualized using differential interference contrast (DIC) microscopy. Whole-cell patch-clamp recordings were obtained using glass microelectrodes (4-6 MΩ resistance, tip size of 3-4 μm). To record intrinsic membrane properties, patch electrodes were filled with intracellular solution containing 130 K-gluconate, 5.5 EGTA, 10 HEPES, 2 NaCl, 2 KCl, 0.5 $CaCl_2$, 0.3 Na_2GTP, 2 MgATP, 7 phosphocreatine (concentrations in mM, pH = 7.2, 289-292 mOsm/kg-H_2O). Baseline membrane voltage (resting membrane potential, V_m), as well as membrane voltage responses to 20pA current injection steps (from -100 to +400pA, 500ms duration), were recorded. Spontaneous excitatory and inhibitory postsynaptic currents (sE/IPSCs) were recorded using patch pipettes containing 130 $CsMeSO_4$, 3 CsCl, 10 HEPES, 2 MgATP, 0.3 Na_2GTP, 5 EGTA, 10 Phosphocreatine, 5 QX-314, 8 biocytin (Concentration in mM; pH 7.2, 291-294 mOsm/kg-H_2O). Excitatory and inhibitory currents were isolated by clamping neuronal membrane potential to -70mV (near inhibitory reversal potential) and 10mV (near excitatory reversal potential) respectively. EPSCs and IPSCs were pharmacologically blocked by DNQX (50 μM) and picrotoxin (PTX, 20 μM) respectively, confirming the AMPA and $GABA_A$ receptor-mediated nature of the respective currents.

Tonic inhibitory current recording

To isolate tonic inhibitory currents, $GABA_A$ receptor-mediated phasic IPSCs were suppressed using 20 µM PTX for at least 5 minutes.[22,23] A histogram of 10,000 data points (5 sec at 2KHz) was generated at baseline and after PTX treatment. A gaussian filter was fitted to the part of the distribution not skewed by phasic IPSCs to obtain mean holding currents.[22] The PTX-sensitive tonic current was measured by subtracting the mean holding currents following PTX treatment from the baseline.

Stimulus train evoked E/IPSCs

For stimulus train experiments, bipolar stimulation electrodes were fabricated from pulled theta glass pipettes (0.5 to 1GΩ resistance, 4-7 µm tip diameter) and filled with saline. Chlorinated silver wires were inserted into each half of the theta glass, and connected to the two poles of the stimulus isolator. Distinct barrels in the L4 somatosensory cortex were identified using IR-DIC microscopy.[24] Theta glass stimulation electrodes were placed at the bottom edge of the barrels. Postsynaptic L2/3 neurons from the same cortical column were patched for voltage-clamp recordings. Postsynaptic responses to 100 µs stimuli ranging from 1 to 10 mV intensity were recorded to establish input-output relationships. The range of stimulus intensity was restricted to evoke only column-specific monosynaptic EPSC (at -70mV) and di-synaptic IPSC (at 10mV) responses. Paired-pulse ratios (PPRs) were calculated as the ratio of amplitudes of the second and the first evoked response (EPSC2/1, Figure 4). Stimulus intensity sufficient to evoke ~50% of the maximum responses was selected for the rest of the experiment. Trains of 10 or 30 stimuli were introduced at different frequencies (10/20/50 Hz) and resulting monosynaptic EPSC and di-synaptic IPSC responses were measured by clamping post-synaptic cell voltage at -70mV and 10mV respectively.[25]

In vivo whole-cell electrophysiology

Mice (males; 2-3 months old) were anesthetized using urethane (0.75 g/kg; i.p.) supplemented with isoflurane (~0.5 %). Body temperature was monitored and maintained at 35 - 37°C using a heating pad. Vital signs (HR: 470–540 bpm, SpO_2: 92-98%, respiration: 120-140/min) were monitored (MouseStat, Kent Scientific) throughout the experiment, and maintained within a physiologically normal range. An Omega-shaped head bar was mounted on the skull, using glue and dental cement, and affixed with screws to a holding rod attached to the stage. A craniotomy 2 mm in diameter was made above the hind paw region of the somatosensory cortex (1 mm caudal to the bregma and 2 mm lateral to the midline), and filled with 1.5% agarose (in

ACSF) to keep the cortical surface moist and dampen the movement associated with breathing.[21] We used *in vivo* whole-cell techniques to record the membrane potential from layer 2/3 pyramidal neurons in the primary somatosensory cortex (S1 L2/3 neurons) and analyzed spontaneous up states in current-clamp mode at resting membrane potential (i.e., -65 to -70 mV). Patch electrodes with 4-6 MΩ resistance and longer taper were used (tip size of 3-4 μm).[21]

2-photon laser scanning microscopy

Acute slices containing the somatosensory cortex were prepared and incubated similarly to whole-cell electrophysiology experiments. After incubation, slices were placed in a submerged chamber and perfused with ACSF (2 to 2.5 mL/min), under a 2-photon microscope (Neurolabware with Hamamatsu H11901 and H10770B photomultiplier tubes; Cambridge Technology CRS8 8KHz resonant scanning mirror and 6215H galvanometer scanning mirror; Nikon 16x/0.8 NA objective; Coherent Cameleon Discovery dual laser system [tunable laser = 920 nm; fixed laser = 1040 nm; pulse width ≈100 fs]; Semrock emission filters [510/84 nm green & 607/70 nm red]; power ≤ 25 mW; 250 μm – 1.5 mm field of view (FOV) on its long axis with ~1.15-1.73μm/pixel resolution at 2X digital zoom, Scanbox acquisition software). Glutamate transients were evoked using a stimulation paradigm similar to the whole-cell electrophysiology experiments, in the presence of glutamate receptor antagonists (CNQX 20μM, AP5 50μM).[26] Maps of glutamate transients across layers were acquired by scanning the entire field of view (512 lines/frame) at 15.49 Hz. After confirming a measurable stimulus-evoked response (>mean+(3*SD) of baseline), L2/3 glutamate transients were temporally resolved using limited area scans (100 lines/frame at 79.80 Hz).

Data quantification and analysis.

Whole-cell electrophysiology

All recordings were acquired at 20kHz and filtered at 2kHz (lowpass) using a Multiclamp 700B amplifier. Analog data were digitized using Digidata 1330 digitizer and Clampex 9 software (Axon Instruments). Access resistance was monitored throughout recordings (5mV pulses at 50Hz). Recordings with access resistance higher than 25MΩ or with > 20% change in the access resistance were discarded from the analysis. 70% series resistance compensation was applied to recorded currents in the voltage-clamp setting. Offline data processing was done with Clampfit 10 (Axon Instruments).

Stimulus-evoked glutamate transients

Image stacks were converted to maximum intensity projections and regions of interest (ROIs) were determined using a binary map of all pixels with a grayscale value > 2X standard deviation of maximum intensity projection (avoiding the slice anchor and stimulation electrode if these present within the FOV). The mean fluorescence intensities of the initial 50 frames of each trial served as F_0. Fluorescence intensity traces were collected as the average intensity of all pixels within the ROI and normalized as $\Delta F/F_0$. Peak amplitude, the area under the curve (AUC), and full width at the half-maximum response (FWHM) of the glutamate transients were calculated using MATLAB (findpeaks function).

Analysis and statistics

Data analysis was performed using GraphPad Prism 8 (GraphPad Software, San Diego, California), MATLAB R2020a (Mathworks), Stata (StataCorp), and Microsoft Excel (Microsoft Corp). The normality of distributions was determined using the D'Agostino-Pearson K2 test and Shapiro-Wilk test. Outliers were identified based on data distribution (Grubbs' test for parametric data and 1.5*interquartile range for non-parametric data). Average values for individual cells were compared across genotypes using a two-tailed, unpaired t-test (parametric data) or Mann-Whitney U test (non-parametric data). Paired comparisons were done using a two-tailed, paired t-test. Normalized (%) distributions of individual events were compared across genotypes using a two-sample Kolmogorov–Smirnov (KS) test. Data representing multiple time points within the same slice were compared across groups using two-way ANOVA (Friedman's test for non-parametric data) or within groups using one-way ANOVA (Kruskal Wallis test for non-parametric data). For multiple comparisons, Bonferroni's correction or Tukey's test was used post-hoc for equal sample sizes. To compare the kinetics of input current-voltage (I/V) and action potential frequency-input current (F/I) relationships, linear regression was fitted across datasets, and slopes were compared between genotypes. To estimate the size and replenishment rate of the readily releasable pool (RRP), we fitted linear regressions to steady-state cumulative amplitudes of E/IPSCs. Y intercepts (RRP size) and slopes (RRP replenishment rates) of the linear regression fit were measured for grand means for genotypes or individual neurons.[27,28] For pharmacology experiments, comparisons between cells before and after drug treatment within a genotype were done by paired t-test; comparisons between control and drug treatment groups across genotypes were done by two-way ANOVA

with Tukey's post hoc test. Statistical significance was set at $P < 0.05$, $*P < 0.05$, $**P < 0.01$, $***P < 0.001$, $****P < 0.0001$.

Data availability

The authors confirm that the data supporting the findings of this study are available within the article and its supplementary material. Raw data were generated at The University of Utah. Raw and derived data supporting the findings of this study are available on request from the corresponding author.

Results

CK1δ_{T44A} mice have hyperexcitable sensory cortical circuits despite hyperpolarized membrane potentials *in vivo*

Hyperexcitable cortical sensory circuits can render the cortex susceptible to SD[12,13] as well as confer tactile and thermal hypersensitivity[29,30], similar to that observed previously in CK1δ_{T44A} mice.[15] Under anesthesia or in quiet wakefulness, cortical networks can oscillate between depolarized 'up states' and quiescent 'down states'.[31,32] Up/down states are regulated by the balance of excitatory and inhibitory synaptic activity. As such, these states dynamically modulate cortical circuit gain, as neurons are more likely to fire action potentials (APs) during up states and less likely during down states.[32,33] We recorded L2/3 pyramidal neuronal membrane potential (V_m) oscillations during up and down states *in vivo*, to characterize network-driven excitability in WT and CK1δ_{T44A} mice (Figure 1A).

To our surprise, neuronal resting V_m during down states was significantly hyperpolarized (two-tailed t-test, $P<0.01$), in CK1δ_{T44A} mice – which is commonly associated with *reduced* excitability (Figure 1B). However, the duration of individual up states in CK1δ_{T44A} mice was significantly increased (2-sample KS test, $p<0.0001$, Figure 1C), as was the mean durations of all up states per animal (two-tailed t-test, $P<0.05$, Figure 1D). V_m variance, which represents the magnitude of persistent synaptic barrages during up states,[32] was also significantly higher in CK1δ_{T44A} mice (2-sample KS test, $p<0.0001$, Figure 1E), confirming hyperexcitable cortical circuits in CK1δ_{T44A} mice, despite the hyperpolarized resting V_m.

Hyperpolarized membrane potential in CK1δ_{T44A} neurons is due to increased tonic inhibition

For further mechanistic dissection of the circuit phenotypes in CK1δ_{T44A} mice, we used *in vitro* whole-cell electrophysiology in acute cortical slices (Figure 2A). Consistent with our *in vivo* finding, CK1δ_{T44A} neurons were hyperpolarized compared to WT littermates (two-tailed t-test, $P<0.01$, Figure 2B), confirming the viability of brain slice preparation as a platform for more detailed examination.

Tonic inhibitory currents can contribute to neuronal V_m hyperpolarization.[23] We recorded tonic holding currents (holding potential; V_{clamp}: 10mV) before and after blocking $GABA_A$ receptors with 20 μM PTX (Figure 2C). We found that CK1δ_{T44A} neurons had significantly larger PTX-sensitive tonic inhibitory currents compared to WT (Mann Whitney test, $P<0.05$, Figure 2D). To determine if increased tonic inhibitory currents in CK1δ_{T44A} neurons substantially contribute to hyperpolarization, we recorded neuronal resting V_m before and after PTX treatment. As expected, PTX treatment depolarized neuronal resting V_m and reduced rheobase in both WT and CK1δ_{T44A} neurons (Figure 2E, S2). However, PTX-induced depolarization was significantly larger in CK1δ_{T44A} neurons compared to WT (Figure 2F). PTX also rescued neuronal V_m in CK1δ_{T44A} neurons (two-way ANOVA, Figure 2G), suggesting that increased tonic inhibition was the primary cause of resting V_m hyperpolarization.

Increased frequency of evoked action potentials due to higher synaptic feedback excitation in CK1δ_{T44A} neurons

Thus far, our results show that CK1δ_{T44A} neurons were hyperpolarized due to increased tonic inhibition, yet there was an increase in cortical circuit excitability *in vivo*. Therefore, we examined whether CK1δ_{T44A} neurons were intrinsically hyperexcitable, by measuring membrane voltage (V_m) responses to a range of input currents (Figure 3A). There was no difference in the neuronal membrane resistance (R_m) measured below the action potential (AP) threshold (Figure S1), or the rheobase between the genotypes (Figure 3D). However, in response to larger input currents, CK1δ_{T44A} neurons fired APs at a significantly higher frequency compared to WT neurons (two-way ANOVA, Figure 3B), thus increasing the frequency-input current (FI) slopes in CK1δ_{T44A} neurons (Mann Whitney test, $P<0.05$, Figure 3C). Consistent with the FI slope data, the inter-spike interval between action potentials was significantly shorter in CK1δ_{T44A} neurons at larger input currents (two-way ANOVA, Figure

3H-J). Interestingly, there was no difference in AP half-width and after-hyperpolarization amplitude between the genotypes (Figure 3E-G), suggesting that altered AP kinetics did not contribute to the increased firing in CK1δ_{T44A} neurons. To determine a possible effect of increased tonic inhibition on suprathreshold activity in CK1δ_{T44A} neurons, we recorded evoked APs before and after PTX treatment (Figure 2E) and found no significant difference in FI slopes after PTX treatment in either genotype (Figure S2).

Neuronal action potential bursts elicited by >500ms long input currents, typically used in slice electrophysiology paradigms,[34,35] can generate synaptic feedback excitatory currents within neocortical microcircuits.[36] To test whether recurrent feedback excitation contributes to increased firing frequency in CK1δ_{T44A} neurons, we recorded evoked APs in the presence of ionotropic glutamate receptor antagonists (AMPARs and NMDARs) to abolish postsynaptic excitatory currents (Figure 3K). Glutamate receptor antagonists normalized the elevated AP frequency (two-way ANOVA, Figure 3L) and larger FI curve slopes in CK1δ_{T44A} neurons (two-tailed t-test, Figure 3M). Therefore, increased feedback synaptic excitation facilitated a higher frequency of evoked APs at larger input currents, suggesting that elevated excitatory synaptic activity may underlie the increased cortical excitability in CK1δ_{T44A} neurons.

Baseline phasic excitatory and inhibitory neurotransmission is unaffected in CK1δ_{T44A} neurons

Balanced synaptic excitation and inhibition mediate "normal" cortical circuit excitability.[32,37] We next examined whether baseline excitatory and inhibitory synaptic transmission contributed to hyperexcitability in CK1$_{\delta T44A}$ circuits. We recorded AP-independent miniature excitatory and inhibitory postsynaptic currents (mE/IPSCs) in the presence of 1μM TTX (Figure S3A, S3B). We found that neither mEPSC amplitude nor frequency was significantly different between WT and CK1δ_{T44A} neurons (two-tailed t-test, Figure S3C, S3E). Similarly, mIPSC amplitude and frequency were not different between the genotypes (two-tailed t-test, Figure S3D, S3F). We found no difference in AP-dependent spontaneous excitatory and inhibitory neurotransmission (Figure S4). Finally, we recorded evoked E/IPSCs in L2/3 neurons in response to a single stimulus in layer 4 (L4). Again, we found no difference in the E/IPSC amplitude ratio between the genotypes (two-tailed t-test, Figure S4H).

NMDA receptor-mediated currents are a key component of excitatory neurotransmission and are modulated through phosphorylation by CK1 family proteins.[38] To test if NMDA receptor-

mediated currents were altered in CK1δ_{T44A} mice, we calculated the ratio of NMDA and AMPA components of responses (AMPA/NMDA ratio) evoked by a single stimulus (L4 to L2/3). We observed no significant difference in the AMPA/NMDA ratio in CK1δ_{T44A} compared to WT neurons (two-tailed t-test, Figure S4I). Taken together, our results suggest that neither phasic excitatory nor inhibitory synaptic transmission was altered in CK1δ_{T44A} neurons.

Frequency-dependent adaptation deficit at CK1δ_{T44A} excitatory synapses

Thus far, we found that CK1δ_{T44A} mice exhibit an increase in local circuit excitability, yet there are no changes in phasic excitatory or inhibitory neurotransmission. We reasoned that this might be due to an altered postsynaptic response of CK1δ_{T44A} neurons to sustained synaptic stimulation.[32,39] To test this, we recorded evoked E/IPSCs following short stimulus trains (L4-L2/3, 10 or 30 stimuli) at different frequencies (10, 20, 50Hz) (Figure 4A-B). To avoid polysynaptic responses, we verified the response latency and column-specificity of stimuli by confirming a lack of evoked responses outside the cortical column (Figure S7).

WT synapses showed the expected adaptation of postsynaptic responses to trains of 30 stimuli, as well as a paired-pulse ratio (PPR) consistent with that described in the literature for adult L4-L2/3 primary sensory cortex synapses.[40] CK1δ_{T44A} neurons showed a similar response to WT at 10Hz stimulation. However, as stimulus frequency increased, the evoked EPSC adaptation showed a weak attenuation at 20Hz, a robust and significant reduction at 50Hz, (Two-way ANOVA, Figure 4C-E), and a significant increase in PPR (two-tailed t-test, Figure 4E, *inset*). We observed a similar frequency-dependent adaptation deficit in CK1δ_{T44A} EPSCs, following shorter duration (10 stimuli) trains (Figure S8). Interestingly, the impaired adaptation in CK1δ_{T44A} neurons was specific to excitatory currents, with evoked inhibitory currents exhibiting adaptation and PPR similar to WT at all stimulation frequencies (Two-way ANOVA, Figure S6A-C). Taken together, these results suggest a reduced adaptation of excitatory currents in CK1δ_{T44A} neurons following repeated high-frequency stimuli.

Increased size of readily releasable pool impairs CK1δ_{T44A} excitatory synaptic adaptation

The rapid adaptation of excitatory postsynaptic currents is due to a presynaptic phenomenon involving Ca^{2+}-mediated depletion and replenishment of the RRP of synaptic vesicles.[41] The

RRP size and its rate of replenishment influence the adaption of postsynaptic responses.[27,42,43] We used the approach initially described by Schneggenburger *et al.*[44–46] in the Calyx of Held, which was later adapted to cortical synapses by Abrahamsson *et al.*,[47] to explore the components of the presynaptic release machinery that contribute to the reduced adaptation at CK1δ_{T44A} synapses. This model uses cumulative postsynaptic current amplitude as a function of stimulus number, with the slope of linear extrapolation of the steady-state indicating the RRP replenishment rate and the y-intercept corresponding to the RRP size (Figure 4F, G)[47].

For EPSCs, there was no difference in the linear regression slope (replenishment rate) between genotypes at any of the frequencies tested. At 10Hz there was no difference in y-intercept (RRP size); however, at both 20Hz and 50Hz, there was a significant increase in the y-intercepts (more robust at 50Hz), consistent with a frequency-dependent increase in RRP size in CK1δ_{T44A} compared to WT animals (ANCOVA, $P<0.0001$, unpaired t-test, $p<0.05$, Figure 4H-M).

In contrast, neither replenishment rate nor RRP size was different for IPSC amplitudes between WT and CK1δ_{T44A} at any stimulus frequency (Figure S6D-I), confirming no difference in presynaptic adaptation at inhibitory synapses. These data predict that a larger presynaptic RRP during high-frequency stimulation at CK1δ_{T44A} glutamatergic synapses is responsible for the observed adaptation deficit.

The adaptation deficit at CK1δ_{T44A} excitatory synapses is $[Ca^{2+}]_e$ dependent.

Recent evidence suggests that the RRP is a subset of fusion-competent and primed vesicles that may or may not be docked.[27] Vesicle docking, priming, and release are Ca^{2+}-dependent mechanisms, often modulated by extracellular $[Ca^{2+}]$,[44,47] that ultimately determine the RRP size.[48,49] Following high-frequency stimulation, residual Ca^{2+} and subsequent activation of biochemical cascades enhance vesicle priming and fusion, increasing the RRP size.[50] We next tested whether increased RRP size at CK1δ_{T44A} glutamatergic synapses following high-frequency stimulation was dependent on $[Ca^{2+}]_e$. We evoked EPSC responses to stimulus trains (10, 20, and 50Hz) in the presence of low Ca^{2+} ACSF (0.65mM vs. 1.3mM in normal ACSF; Figure 5A, B). We found that the adaptation deficit at CK1δ_{T44A} excitatory synapses following 50Hz stimulation was 'normalized' with low Ca^{2+} ACSF (two-way ANOVA, Figure 5E), with RRP size (unpaired t-test, Figure 5I) and replenishment rate (unpaired t-test, Figure 5J) similar

to WT levels. Therefore, the adaptation deficit at CK1δ_{T44A} excitatory synapses is dependent on $[Ca^{2+}]_e$, consistent with a presynaptic RRP-dependent mechanism.

Larger glutamate transients following high-frequency stimulation in CK1δ_{T44A} slices

Our data thus far implicate that a larger RRP size at glutamatergic synapses during repeated high-frequency stimulation results in reduced adaptation. A larger RRP size would likely entail an increase in glutamate release, which can be measured with fluorescent indicators.[51] Employing an approach similar to that described by Armbruster *et al*.,[26] we imaged glutamate transients in L2/3 upon stimulation of L4 afferents, using two-photon laser-scanning microscopy (Figure 6A-B).

Glutamate signals were evoked using a stimulation paradigm similar to that used for electrophysiology experiments. Glutamate maps acquired by scanning the entire field of view (at 15.49 Hz) showed a column-specific distribution of evoked responses, similar to evoked EPSC recordings (Figure S7, Movie S1). L2/3 glutamate transients in the appropriate column were then temporally resolved by faster limited-area scans (79.80 Hz at 100 lines/frame, Movie S2, *Materials and Methods*). Glutamate transients evoked in L2/3 in response to 10Hz and 20Hz stimulus trains were not significantly different between genotypes (Mann Whitney test, Figure 6C-F). However, there was a significant increase in peak amplitude and area under the curve (AUC) of glutamate transients in CK1δ_{T44A} slices compared to WT during 50Hz stimulations (Mann Whitney test, Figure 6G-H), suggesting increased glutamate release[52,53] following high-frequency stimulation of CK1δ_{T44A}cortical synapses. This finding offers convergent evidence of a presynaptic gain of function as a key underlying mechanism and a potential bridge between the cellular and circuit CK1δ_{T44A} phenotypes.

An excitatory shift in the cortical circuits of CK1δ_{T44A} mice, *in vitro* and *in vivo*.

Reduced adaptation at excitatory, but not inhibitory synapses, can result in a net excitatory shift in cortical microcircuits following stimulation, especially given the finding that reduced synaptic adaptation is associated with increased glutamate release. To test this hypothesis, we generated E/I ratios by measuring the amplitude of evoked E/IPSCs during stimulus trains (10 stimuli) recorded from the same neurons (Figure 7A). As expected, we observed a significant

excitatory shift in CK1δ_{T44A} neurons after 50Hz stimulation (two-way ANOVA, $p<0.05$), but not at 20 or 10Hz (Figure 7B-D). We then tested whether the net excitatory shift upon intense synaptic stimulation is preserved in intact neural networks *in vi*vo (Figure 7E). During up states, cortical neurons exhibit both excitatory and inhibitory synaptic barrages when recorded using voltage-clamp electrophysiology *(Materials and Methods)*. We observed a robust increase in the duration of up-state evoked excitatory currents (Figure 7G), without a significant difference in the duration of inhibitory currents (Figure 7F), consistent with reduced adaptation observed exclusively at glutamatergic synapses in brain slices. Therefore, intense activity results in an excitatory shift in the output of cortical synapses *in vitro* and *in vivo,* in CK1δ_{T44A} mice.

Reduced $[Ca^{2+}]_e$ normalizes SD susceptibility in CK1δ_{T44A} slices.

CK1δ_{T44A} mice exhibit increased susceptibility to experimental SD induction *in vivo.*[15] Similar observations of SD susceptibility in other migraine models are attributed to the increased release probability,[13] or impaired clearance,[14] of glutamate. To test whether the glutamatergic gain of function due to impaired adaptation at CK1δ_{T44A} excitatory synapses results in the facilitation of SD, we measured the threshold for SD induction *(Materials and Methods)* in acute cortical slices (Figure 7H, Movie S3). As expected, the threshold for SD initiation was significantly reduced in CK1δ_{T44A} slices compared to WT littermates (two-way ANOVA, Figure 7I).

To determine whether impaired adaptation at glutamatergic synapses had a causal role in the threshold difference, we measured SD thresholds in WT and CK1δ_{T44A} slices perfused with low Ca^{2+} ACSF, with the rationale that the reduced adaptation in CK1δ_{T44A} slices was $[Ca^{2+}]_e$ dependent (Figure 5). As SD induction itself depends on $[Ca^{2+}]_e$,[55] low $[Ca^{2+}]_e$ significantly increased the SD threshold in slices from *both* genotypes, along with reduced maximum SD propagation (Figure S9). However, a comparison between genotypes in low $[Ca^{2+}]_e$ conditions revealed a 'rescue' of reduced SD thresholds in CK1δ_{T44A} slices (two-way ANOVA, Figure 7I) suggesting a $[Ca^{2+}]_e$ mediated mechanism underlies the reduced threshold in CK1δ_{T44A} compared to WT. Taken together, our results demonstrate that $[Ca^{2+}]_e$-mediated presynaptic adaptation deficit at excitatory synapses likely contributes to cortical network hyperexcitability and SD susceptibility in CK1δT44A mice (Figure 8).

Discussion

Despite the pervasive and debilitating nature of migraine, the underlying mechanisms remain poorly understood.[1,2] In CK1δ_{T44A} mice expressing a mutation found in humans with migraine with aura, we found a calcium-dependent reduction in presynaptic adaptation (Figure 4) and increased release (Figure 6) exclusively at glutamatergic synapses following intense circuit stimulation. This occurred despite increased tonic inhibition (Figure 2) as well as normal subthreshold and synaptic activity (Figure S1-S4). The stimulus-dependent increase in excitability bears an intriguing resemblance to migraine symptom descriptions and electrophysiological phenotypes in humans,[7,56,57] and it provides a synaptic and circuit mechanism for the increased cortical excitability noted in CK1δ_{T44A} mice (Figure 1).[15] Finally, we show a $[Ca^{2+}]_e$ -dependent increase in SD susceptibility CK1δ_{T44A} slices (Figure 7), directly implicating $[Ca^{2+}]_e$-dependent presynaptic mechanisms in migraine-relevant circuit excitability (Figure 8).[13,55]

Although migraine is more commonly polygenic,[3] animal models of monogenic forms of the disorder offer a unique opportunity for mechanistic dissection.[12–14,58,59] Recently, a loss of function mutation in the casein kinase 1 delta gene (CK1δ_{T44A}) was identified in two families with a combination of familial migraine with aura and advanced sleep phase syndrome.[15,20] Mice harboring this mutation showed migraine-relevant network excitability phenotypes including increased SD susceptibility and tactile and thermal hyperalgesia. These phenotypes were associated with increased c-fos expression in the trigeminal nucleus caudalis after administration of the migraine-triggering drug nitroglycerin.[15] SD-associated vascular responses were also heightened in CK1δ_{T44A} mice. As SD likely triggers craniofacial pain at least partly through activation of vascular afferents,[9,60] this phenotype might be evidence of a larger perturbation of pain-sensitive structures. The combined cortical excitability, vascular, and pain phenotypes in CK1δ_{T44A} mice,[15] strongly argue for its broad disease relevance, despite the rarity of the mutation.

Sensory amplifications, during and between attacks, are a key feature of migraine.[61–63] Sensory amplifications correlate with headache frequency and disease severity[64–66] and are associated with poor clinical outcomes.[67] Interestingly, migraineurs also report a lack of habituation to repeated sensory stimuli.[8,68–70] Presynaptic adaptation is one of the principal mechanisms regulating sensory habituation and gain modulation in sensory circuits.[71,72] In the cortex, a precise balance between synaptic excitation and inhibition is important for establishing the

timing and signal-to-noise ratio necessary for signal processing.[73] Stimulus-evoked and spontaneous activity in the sensory cortex involves a stereotypical pattern of excitation followed by inhibition.[74–76] Even under normal conditions, synaptic excitation adapts more slowly than inhibition following repeated stimulation in the sensory cortex,[77,78] generating a temporal window for the sensory signal integration.[24,79] Reduced adaptation at excitatory – but *not* inhibitory - synapses upon high-frequency stimulation in CK1δ_{T44A} cortical neurons can thus significantly enhance signal transmission, resulting in sensory amplification.

Our findings are quite consistent with a scenario of enhanced cortical excitation due to the selective deficit in the adaptation of CK1δ_{T44A} excitatory neurons. The adaptation deficit is caused and accompanied by increased glutamate release. Increased glutamate release is a likely reason for the glutamate-dependent increase in feedback excitation we observed upon high-frequency stimulation (Figure 3). It also likely accounts for the increased up-state duration and membrane potential variance (Figure 1), which represents local synaptic barrages during depolarized up-states.

Interestingly, impaired adaptation is also present in other genetic models of migraine (FHM1)[80,81] and it also occurs after SD,[82] potentially providing a common presynaptic mechanism for the habituation failure to repeated stimuli reported in migraineurs.[7] However, it is also important to note differences between the gain phenotypes in different models, as these may also have clinical relevance. The presynaptic gain of function phenotype in FHM1 differs from that of the CK1δ_{T44A} model, as a single stimulus is sufficient to elicit larger amplitude postsynaptic excitatory responses in FHM1.[13] In the case of the CK1δ_{T44A} mouse model, repetitive high-frequency stimuli are necessary to elicit a glutamatergic adaptation deficit. Similarly, astrocytic transporter currents evoked by single stimuli, that represent the rate of glutamate clearance, are slower in FHM2 mice.[14] This appears to correlate with the differences in the severity of disease between FHM syndromes (associated with hemiplegic or paralytic auras) and CK1δ_{T44A} mutation carriers, who report the non-hemiplegic auras which are also more common in the general migraine population.[3,11] The response to repetitive rather than single stimulation is also consistent with patient reports of triggering migraines with high-intensity sensory inputs.[8,69]

Sensory perception is a multi-synaptic, multi-circuit process, and the mechanisms underlying altered perception extend well beyond the single-synapse level. Therefore, understanding migraine as a disorder of sensory gain requires an examination of circuit-wide mechanisms *in*

vivo. Cortical slow oscillations are a well-characterized form of dynamic gain modulation in sensory circuits:[83] depolarized 'up states' increase the likelihood of AP generation,[33,84] and have been proposed as coincidence detectors for feedforward signal transmission[85] during quiet wakefulness. Interestingly, increased up state frequency and duration have also been reported as a marker for network excitability in epilepsy models.[86,87] Both migraine and epilepsy patients show alterations in high- and low-frequency cortical and thalamocortical oscillations, and the low-frequency oscillations are proposed as correlates of up states.[32,56,88] Up state phenotypes thus provide a cortical circuit mechanism that can potentially bind the phenotypes observed in both humans and animal models of migraine.

Our *in vivo* investigations of cortical slow oscillations showed increased up-state duration and membrane voltage variance in CK1δ_{T44A} mice, despite hyperpolarized resting membrane potentials at baseline. During up-states, we found that CK1δ_{T44A} neurons received excitatory post-synaptic currents for a significantly longer duration than WT neurons, tipping the excitatory-inhibitory balance towards excitation. These *in vivo* findings bear an interesting resemblance to the increased frequency of action potentials evoked using intense stimuli *in vitro* in CK1δ_{T44A} neurons as both phenomena are dependent on glutamatergic input and rely on local feedback excitation. Since up states are *spontaneous* rather than evoked events that can occur during quiet wakefulness,[32] CK1δ_{T44A} circuits may be hyperexcitable at baseline, without exposure to repetitive high-intensity stimuli.

At the synaptic level, our results showed a Ca^{2+}-dependent increase in RRP size in CK1δ_{T44A} mice following high-frequency stimulation at excitatory synapses. The RRP is functionally defined as a subset of fusion-competent and primed vesicles in a presynaptic bouton that are more easily released than the remaining vesicle population.[27,48,49] The RRP is thus dynamic, and its size changes as it is depleted and replenished simultaneously during repeated stimulation.[27] This dynamic modulation of RRP size is dependent on $[Ca^{2+}]_e$[44,46] as well as stimulus frequency.[89,90] An increase in RRP size, as we observe in CK1δ_{T44A} on intense stimulation, has been shown to increase stimulus-evoked release probability,[89] which can enhance Ca^{2+} -dependent glutamate release.[91]

The high-frequency stimulus-dependent increase we observed in the RRP of CK1δ_{T44A} synapses prompts a comparison with post-tetanic potentiation (PTP), which is attributed to elevated residual Ca^{2+}, or changes to release machinery, including vesicle priming.[42,92] Residual Ca^{2+} following high-frequency stimulation has been shown to activate biochemical

targets like protein kinase C, Munc13, synapsin, and calmodulin/CaM kinase II, all of which regulate the size of the RRP.[93–95] Post-tetanic potentiation is dependent on enhanced Ca^{2+} sensitivity of the vesicle fusion process, mediated by protein kinase C and Munc13.[93,94] Moreover, genetic manipulations that impair RIM- and Munc13- mediated vesicle priming affect the RRP size.[27,96,97] Interestingly, CK1 kinases co-localize with synaptic vesicular markers and phosphorylate a subset of synaptic vesicle-associated proteins (SV2). [18] Phosphorylation of $SV2_A$ protein by CK1 family kinases controls the retrieval of synaptotagmin-1, a calcium sensor for the SNARE complex mediating the release of synaptic vesicles.[28,98]

Development-dependent morphological changes in synapses can also affect vesicle release probability. Recent evidence from CK1δ loss of function mutants in C. elegans suggests a potential role in axon maturation and stabilization.[99] Multiple studies have demonstrated the variations in the presynaptic RRP size and release efficacy at different stages of axonal maturation.[100,101] Therefore, a developmental role of the kinase in $CK1\delta_{T44A}$ mice could contribute to the presynaptic phenotypes observed in this study.[18] Taken together, these findings support a possible role of CK1δ in the regulation of presynaptic function and suggest avenues for further investigation to uncover the molecular mechanisms responsible for the $CK1\delta_{T44A}$ adaptation phenotype. Moreover, the reduced thresholds for SD induction in $CK1\delta_{T44A}$ acute slices were normalized by low extracellular Ca^{2+} (Figure 7), elucidating a functional link between presynaptic facilitation and migraine-relevant circuit excitability.

Intriguingly, we observed an increase in the tonic inhibitory currents of $CK1\delta_{T44A}$ neurons, leading to a hyperpolarized resting V_m, which is generally consistent with a *reduction* in excitability. At first approximation, this result appears to counter the other cellular and circuit phenotypes and suggests a possible compensatory mechanism. However, there is an equally tenable alternative explanation. Tonic inhibitory currents are mediated by extra and peri-synaptic $GABA_A$ receptors[23] and can be elicited by low levels of ambient GABA, due to their high GABA affinity.[22,102] Tonic inhibitory currents are modulated by vesicular GABA release as well as reuptake, and therefore their activity correlates with the intensity of local network activity.[22,103] Under baseline conditions, GABA transporters responsible for reuptake remain close to equilibrium (reversal) potential.[104] As a result, even moderate circuit activity (brief neuronal depolarization or bursts of action potentials) is sufficient for GABA transporter reversal, resulting in both vesicular as well as non-vesicular GABA release,[105,106] both of which can contribute to tonic inhibitory currents.[107] Thus, a plausible explanation of the increased

tonic inhibitory currents in CK1δ_{T44A} neurons is that they are a direct *consequence* of the hyperexcitable cortical circuits wrought by the presynaptic gain of function, rather than a compensatory response. It should also be considered that tonic inhibition may even *contribute* to network excitability, as the resulting increase in $[Cl^-]_i$ can render GABA excitatory, due to depolarized GABA reversal potential.[108–110] That said, tonic inhibition as a more regulated compensatory response to circuit excitability (e.g. via reductions in GABA transporter expression)[111] cannot be ruled out. Ultimately, despite the increased tonic inhibition, CK1δ_{T44A} cortical circuits remain hyperexcitable.

In conclusion, we uncovered evidence of a presynaptic gain of function at glutamatergic synapses in CK1δ_{T44A} mice, due to a calcium-dependent increase in RRP size that results in increased synaptic glutamate release. This gain of function caused a stimulus-dependent adaptation deficit of glutamatergic synaptic activity and was accompanied by enhanced network activity both *in vitro* and *in vivo,* that contributed to SD susceptibility. Taken together, our findings in CK1δ_{T44A} mice confirm presynaptic origins of cortical circuit excitability associated with phenotypically common form of migraine (Figure 8).

Acknowledgements

We thank Drs. Jeremy Theriot, Patrick Parker, and Kate Reinhart for providing technical direction; Loren L. Looger, and the Howard Hughes Medical Institute for providing iGluSnFR reagents to the research community.

Funding

This work was supported by the National Institutes of Health: R01 NS102978 and NS104742; DoD PR200891 (K.C.B.).

Competing interests

The authors have no conflict of interest to declare.

Supplementary material

Supplementary material is available at *Brain* online

References

1. Stewart WF, Ricci JA, Chee E, Morganstein D, Lipton R. Lost productive time and cost due to common pain conditions in the US workforce. *JAMA*. 2003;290(18):2443-2454. doi:10.1001/jama.290.18.2443

2. Lipton RB, Bigal ME, Diamond M, et al. Migraine prevalence, disease burden, and the need for preventive therapy. *Neurology*. 2007;68(5):343-349. doi:10.1212/01.wnl.0000252808.97649.21

3. Brennan KC, Pietrobon D. A Systems Neuroscience Approach to Migraine. *Neuron*. 2018;97(5):1004-1021. doi:10.1016/j.neuron.2018.01.029

4. Mulleners WM, Aurora SK, Chronicle EP, Stewart R, Gopal S, Koehler PJ. Self-reported photophobic symptoms in migraineurs and controls are reliable and predict diagnostic category accurately. *Headache*. 2001;41(1):31-39.

5. Lipton RB, Bigal ME, Ashina S, et al. Cutaneous allodynia in the migraine population. *Ann Neurol*. 2008;63(2):148-158. doi:10.1002/ana.21211

6. Ambrosini A, Schoenen J. Electrophysiological response patterns of primary sensory cortices in migraine. *J Headache Pain*. 2006;7(6):377-388. doi:10.1007/s10194-006-0343-x

7. Coppola G, Pierelli F, Schoenen J. Habituation and migraine. *Neurobiol Learn Mem*. 2009;92(2):249-259. doi:10.1016/j.nlm.2008.07.006

8. Coppola G, Schoenen J. Cortical excitability in chronic migraine. *Curr Pain Headache Rep*. 2012;16(1):93-100. doi:10.1007/s11916-011-0231-1

9. Pietrobon D, Moskowitz MA. Chaos and commotion in the wake of cortical spreading depression and spreading depolarizations. *Nat Rev Neurosci*. 2014;15(6):379-393. doi:10.1038/nrn3770

10. Perlman RL. Mouse models of human disease. *Evol Med Public Health*. 2016;2016(1):170-176. doi:10.1093/emph/eow014

11. Pietrobon D. Familial hemiplegic migraine. *Neurotherapeutics*. 2007;4(2):274-284. doi:10.1016/j.nurt.2007.01.008

12. van den Maagdenberg AMJM, Pietrobon D, Pizzorusso T, et al. A Cacna1a knockin migraine mouse model with increased susceptibility to cortical spreading depression. *Neuron*. 2004;41(5):701-710. doi:10.1016/s0896-6273(04)00085-6

13. Tottene A, Conti R, Fabbro A, et al. Enhanced excitatory transmission at cortical synapses as the basis for facilitated spreading depression in Ca(v)2.1 knockin migraine mice. *Neuron*. 2009;61(5):762-773. doi:10.1016/j.neuron.2009.01.027

14. Capuani C, Melone M, Tottene A, et al. Defective glutamate and K+ clearance by cortical astrocytes in familial hemiplegic migraine type 2. *EMBO Mol Med*. 2016;8(8):967-986. doi:10.15252/emmm.201505944

15. Brennan KC, Bates EA, Shapiro RE, et al. Casein Kinase Iδ Mutations in Familial Migraine and Advanced Sleep Phase. *Sci Transl Med*. 2013;5(183):183ra56-11. doi:10.1126/scitranslmed.3005784

16. Etchegaray JP, Machida KK, Noton E, et al. Casein Kinase 1 Delta Regulates the Pace of the Mammalian Circadian Clock. *Molecular and Cellular Biology*. 2009;29(14):3853-3866. doi:10.1128/MCB.00338-09

17. Greer YE, Gao B, Yang Y, Nussenzweig A, Rubin JS. Lack of Casein Kinase 1 Delta Promotes Genomic Instability - The Accumulation of DNA Damage and Down-Regulation of Checkpoint Kinase 1. *PLOS ONE*. 2017;12(1):e0170903. doi:10.1371/journal.pone.0170903

18. Knippschild U, Gocht A, Wolff S, Huber N, Löhler J, Stöter M. The casein kinase 1 family: participation in multiple cellular processes in eukaryotes. *Cell Signal*. 2005;17(6):675-689. doi:10.1016/j.cellsig.2004.12.011

19. Wolff S, Stöter M, Giamas G, et al. Casein kinase 1 delta (CK1δ) interacts with the SNARE associated protein snapin. *FEBS Letters*. 2006;580(27):6477-6484. doi:10.1016/j.febslet.2006.10.068

20. Xu Y, Padiath QS, Shapiro RE, et al. Functional consequences of a CKIdelta mutation causing familial advanced sleep phase syndrome. *Nature*. 2005;434(7033):640-644. doi:10.1038/nature03453

21. Sawant-Pokam PM, Suryavanshi P, Mendez JM, Dudek FE, Brennan KC. Mechanisms of Neuronal Silencing After Cortical Spreading Depression. *Cereb Cortex*. 2017;27(2):1311-1325. doi:10.1093/cercor/bhv328

22. Glykys J, Mody I. The main source of ambient GABA responsible for tonic inhibition in the mouse hippocampus. *J Physiol (Lond)*. 2007;582(Pt 3):1163-1178. doi:10.1113/jphysiol.2007.134460

23. Farrant M, Nusser Z. Variations on an inhibitory theme: phasic and tonic activation of GABA(A) receptors. *Nat Rev Neurosci*. 2005;6(3):215-229. doi:10.1038/nrn1625

24. Petersen CCH, Sakmann B. The Excitatory Neuronal Network of Rat Layer 4 Barrel Cortex. *J Neurosci*. 2000;20(20):7579-7586. doi:10.1523/JNEUROSCI.20-20-07579.2000

25. Varela JA, Song S, Turrigiano GG, Nelson SB. Differential Depression at Excitatory and Inhibitory Synapses in Visual Cortex. *J Neurosci*. 1999;19(11):4293-4304. doi:10.1523/JNEUROSCI.19-11-04293.1999

26. Armbruster M, Hanson E, Dulla CG. Glutamate Clearance Is Locally Modulated by Presynaptic Neuronal Activity in the Cerebral Cortex. *J Neurosci*. 2016;36(40):10404-10415. doi:10.1523/JNEUROSCI.2066-16.2016

27. Kaeser PS, Regehr WG. The readily releasable pool of synaptic vesicles. *Curr Opin Neurobiol*. 2017;43:63-70. doi:10.1016/j.conb.2016.12.012

28. Zhang N, Gordon SL, Fritsch MJ, et al. Phosphorylation of Synaptic Vesicle Protein 2A at Thr84 by Casein Kinase 1 Family Kinases Controls the Specific Retrieval of Synaptotagmin-1. *J Neurosci*. 2015;35(6):2492-2507. doi:10.1523/JNEUROSCI.4248-14.2015

29. Zhang X, Levy D, Kainz V, Noseda R, Jakubowski M, Burstein R. Activation of central trigeminovascular neurons by cortical spreading depression. *Ann Neurol*. 2011;69(5):855-865. doi:10.1002/ana.22329

30. Zhang X, Levy D, Noseda R, Kainz V, Jakubowski M, Burstein R. Activation of meningeal nociceptors by cortical spreading depression: implications for migraine with aura. *J Neurosci*. 2010;30(26):8807-8814. doi:10.1523/JNEUROSCI.0511-10.2010

31. Timofeev I, Steriade M. Low-frequency rhythms in the thalamus of intact-cortex and decorticated cats. *Journal of Neurophysiology*. Published online December 1, 1996. doi:10.1152/jn.1996.76.6.4152

32. Neske GT. The Slow Oscillation in Cortical and Thalamic Networks: Mechanisms and Functions. *Front Neural Circuits*. 2016;9. doi:10.3389/fncir.2015.00088

33. Anderson JS, Lampl I, Gillespie DC, Ferster D. The contribution of noise to contrast invariance of orientation tuning in cat visual cortex. *Science*. 2000;290(5498):1968-1972. doi:10.1126/science.290.5498.1968

34. Kim KR, Lee SY, Yoon SH, et al. Kv4.1, a Key Ion Channel For Low Frequency Firing of Dentate Granule Cells, Is Crucial for Pattern Separation. *J Neurosci*. 2020;40(11):2200-2214. doi:10.1523/JNEUROSCI.1541-19.2020

35. Tateno T, Harsch A, Robinson HPC. Threshold Firing Frequency–Current Relationships of Neurons in Rat Somatosensory Cortex: Type 1 and Type 2 Dynamics. *Journal of Neurophysiology*. 2004;92(4):2283-2294. doi:10.1152/jn.00109.2004

36. Douglas RJ, Koch C, Mahowald M, Martin KAC, Suarez HH. Recurrent Excitation in Neocortical Circuits. *Science*. 1995;269(5226):981-985.

37. Zucca S, D'Urso G, Pasquale V, et al. An inhibitory gate for state transition in cortex. *eLife*. 6. doi:10.7554/eLife.26177

38. Chergui K, Svenningsson P, Greengard P. Physiological role for casein kinase 1 in glutamatergic synaptic transmission. *J Neurosci*. 2005;25(28):6601-6609. doi:10.1523/JNEUROSCI.1082-05.2005

39. Shao Z, Burkhalter A. Different Balance of Excitation and Inhibition in Forward and Feedback Circuits of Rat Visual Cortex. *J Neurosci*. 1996;16(22):7353-7365. doi:10.1523/JNEUROSCI.16-22-07353.1996

40. Cheetham CEJ, Fox K. Presynaptic development at L4 to l2/3 excitatory synapses follows different time courses in visual and somatosensory cortex. *J Neurosci*. 2010;30(38):12566-12571. doi:10.1523/JNEUROSCI.2544-10.2010

41. Hsu SF, Augustine GJ, Jackson MB. Adaptation of Ca2+-Triggered Exocytosis in Presynaptic Terminals. *Neuron*. 1996;17(3):501-512. doi:10.1016/S0896-6273(00)80182-8

42. Fioravante D, Regehr WG. Short-term forms of presynaptic plasticity. *Curr Opin Neurobiol*. 2011;21(2):269-274. doi:10.1016/j.conb.2011.02.003

43. Guo J, Ge J long, Hao M, et al. A Three-Pool Model Dissecting Readily Releasable Pool Replenishment at the Calyx of Held. *Sci Rep*. 2015;5. doi:10.1038/srep09517

44. Schneggenburger R, Meyer AC, Neher E. Released Fraction and Total Size of a Pool of Immediately Available Transmitter Quanta at a Calyx Synapse. *Neuron*. 1999;23(2):399-409. doi:10.1016/S0896-6273(00)80789-8

45. Schneggenburger R, Sakaba T, Neher E. Vesicle pools and short-term synaptic depression: lessons from a large synapse. *Trends in Neurosciences*. 2002;25(4):206-212. doi:10.1016/S0166-2236(02)02139-2

46. Trommershäuser J, Schneggenburger R, Zippelius A, Neher E. Heterogeneous Presynaptic Release Probabilities: Functional Relevance for Short-Term Plasticity. *Biophys J*. 2003;84(3):1563-1579.

47. Abrahamsson T, Chou CYC, Li SY, et al. Differential Regulation of Evoked and Spontaneous Release by Presynaptic NMDA Receptors. *Neuron*. 2017;96(4):839-855.e5. doi:10.1016/j.neuron.2017.09.030

48. Rizzoli SO, Betz WJ. The Structural Organization of the Readily Releasable Pool of Synaptic Vesicles. *Science*. 2004;303(5666):2037-2039. doi:10.1126/science.1094682

49. Jockusch WJ, Speidel D, Sigler A, et al. CAPS-1 and CAPS-2 Are Essential Synaptic Vesicle Priming Proteins. *Cell*. 2007;131(4):796-808. doi:10.1016/j.cell.2007.11.002

50. Fioravante D, Regehr WG. Short-term forms of presynaptic plasticity. *Curr Opin Neurobiol*. 2011;21(2):269-274. doi:10.1016/j.conb.2011.02.003

51. Marvin JS, Borghuis BG, Tian L, et al. An optimized fluorescent probe for visualizing glutamate neurotransmission. *Nat Methods*. 2013;10(2):162-170. doi:10.1038/nmeth.2333

52. Armbruster M, Dulla CG, Diamond JS. Effects of fluorescent glutamate indicators on neurotransmitter diffusion and uptake. Boudker O, Huguenard J, Rowan MJ, eds. *eLife*. 2020;9:e54441. doi:10.7554/eLife.54441

53. Herde MK, Bohmbach K, Domingos C, et al. Local Efficacy of Glutamate Uptake Decreases with Synapse Size. *Cell Reports*. 2020;32(12):108182. doi:10.1016/j.celrep.2020.108182

54. Adesnik H, Scanziani M. Lateral competition for cortical space by layer-specific horizontal circuits. *Nature*. 2010;464(7292):1155-1160. doi:10.1038/nature08935

55. Tottene A, Urbani A, Pietrobon D. Role of different voltage-gated Ca2+ channels in cortical spreading depression: Specific requirement of P/Q-type Ca2+ channels. *Channels*. 2011;5(2):110-114. doi:10.4161/chan.5.2.14149

56. Coppola G, Ambrosini A, Di Clemente L, et al. Interictal abnormalities of gamma band activity in visual evoked responses in migraine: an indication of thalamocortical dysrhythmia? *Cephalalgia*. 2007;27(12):1360-1367. doi:10.1111/j.1468-2982.2007.01466.x

57. Helling RM, Perenboom MJL, Bauer PR, et al. TMS-evoked EEG potentials demonstrate altered cortical excitability in migraine with aura. *Brain Topogr*. 2023;36(2):269-281. doi:10.1007/s10548-023-00943-2

58. Pettingill P, Weir GA, Wei T, et al. A causal role for TRESK loss of function in migraine mechanisms. *Brain*. 2019;142(12):3852-3867. doi:10.1093/brain/awz342

59. Royal P, Andres-Bilbe A, Ávalos Prado P, et al. Migraine-Associated TRESK Mutations Increase Neuronal Excitability through Alternative Translation Initiation and Inhibition of TREK. *Neuron*. 2019;101(2):232-245.e6. doi:10.1016/j.neuron.2018.11.039

60. Karatas H, Erdener SE, Gursoy-Ozdemir Y, et al. Spreading Depression Triggers Headache by Activating Neuronal Panx1 Channels. *Science*. 2013;339(6123):1092-1095. doi:10.1126/science.1231897

61. Ashkenazi A, Mushtaq A, Yang I, Oshinsky ML. Ictal and interictal phonophobia in migraine—a quantitative controlled study. *Cephalalgia*. 2009;29(10):1042-1048. doi:10.1111/j.1468-2982.2008.01834.x

62. Grossi DB, Chaves TC, Gonçalves MC, et al. Pressure pain threshold in the craniocervical muscles of women with episodic and chronic migraine: a controlled study. *Arq Neuropsiquiatr*. 2011;69(4):607-612. doi:10.1590/s0004-282x2011000500007

63. Cortez MM, Rea NA, Hunter LA, Digre KB, Brennan K. Altered pupillary light response scales with disease severity in migrainous photophobia. *Cephalalgia*. 2017;37(8):801-811. doi:10.1177/0333102416673205

64. Benatto MT, Florencio LL, Carvalho GF, et al. Cutaneous allodynia is more frequent in chronic migraine, and its presence and severity seems to be more associated with the duration of the disease. *Arquivos de Neuro-Psiquiatria*. 2017;75(3):153-159. doi:10.1590/0004-282x20170015

65. Carvalho GF, Vianna-Bell FH, Florencio LL, et al. Presence of vestibular symptoms and related disability in migraine with and without aura and chronic migraine: *Cephalalgia*. Published online April 10, 2018. doi:10.1177/0333102418769948

66. Perenboom MJL, Zamanipoor Najafabadi AH, Zielman R, Carpay JA, Ferrari MD. Quantifying visual allodynia across migraine subtypes: the Leiden Visual Sensitivity Scale. *PAIN*. 2018;159(11):2375-2382. doi:10.1097/j.pain.0000000000001343

67. Seo JG, Park SP. Clinical significance of sensory hypersensitivities in migraine patients: does allodynia have a priority on it? *Neurol Sci*. 2019;40(2):393-398. doi:10.1007/s10072-018-3661-2

68. Ambrosini A, Schoenen J. Electrophysiological response patterns of primary sensory cortices in migraine. *J Headache Pain*. 2006;7(6):377-388. doi:10.1007/s10194-006-0343-x

69. Coppola G, Pierelli F, Schoenen J. Habituation and migraine. *Neurobiol Learn Mem*. 2009;92(2):249-259. doi:10.1016/j.nlm.2008.07.006

70. Aurora SK, Barrodale P, Chronicle EP, Mulleners WM. Cortical Inhibition Is Reduced in Chronic and Episodic Migraine and Demonstrates a Spectrum of Illness. *Headache: The Journal of Head and Face Pain*. 2005;45(5):546-552. doi:10.1111/j.1526-4610.2005.05108.x

71. Lampl I, Katz Y. Neuronal adaptation in the somatosensory system of rodents. *Neuroscience*. 2017;343:66-76. doi:10.1016/j.neuroscience.2016.11.043

72. Wark B, Lundstrom BN, Fairhall A. Sensory adaptation. *Curr Opin Neurobiol*. 2007;17(4):423-429. doi:10.1016/j.conb.2007.07.001

73. Isaacson JS, Scanziani M. How inhibition shapes cortical activity. *Neuron*. 2011;72(2):231-243. doi:10.1016/j.neuron.2011.09.027

74. Higley MJ, Contreras D. Balanced excitation and inhibition determine spike timing during frequency adaptation. *J Neurosci*. 2006;26(2):448-457. doi:10.1523/JNEUROSCI.3506-05.2006

75. Okun M, Lampl I. Instantaneous correlation of excitation and inhibition during ongoing and sensory-evoked activities. *Nature Neuroscience*. 2008;11(5):535-537. doi:10.1038/nn.2105

76. Wilent WB, Contreras D. Dynamics of excitation and inhibition underlying stimulus selectivity in rat somatosensory cortex. *Nature Neuroscience*. 2005;8(10):1364-1370. doi:10.1038/nn1545

77. Heiss JE, Katz Y, Ganmor E, Lampl I. Shift in the Balance between Excitation and Inhibition during Sensory Adaptation of S1 Neurons. *J Neurosci*. 2008;28(49):13320-13330. doi:10.1523/JNEUROSCI.2646-08.2008

78. Gabernet L, Jadhav SP, Feldman DE, Carandini M, Scanziani M. Somatosensory Integration Controlled by Dynamic Thalamocortical Feed-Forward Inhibition. *Neuron*. 2005;48(2):315-327. doi:10.1016/j.neuron.2005.09.022

79. Hull C, Scanziani M. It's about time for thalamocortical circuits. *Nature Neuroscience*. 2007;10(4):400-402. doi:10.1038/nn0407-400

80. Inchauspe CG, Urbano FJ, Di Guilmi MN, et al. Presynaptic CaV2.1 calcium channels carrying familial hemiplegic migraine mutation R192Q allow faster recovery from synaptic depression in mouse calyx of Held. *J Neurophysiol*. 2012;108(11):2967-2976. doi:10.1152/jn.01183.2011

81. Tottene A, Favero M, Pietrobon D. Enhanced Thalamocortical Synaptic Transmission and Dysregulation of the Excitatory–Inhibitory Balance at the Thalamocortical Feedforward Inhibitory Microcircuit in a Genetic Mouse Model of Migraine. *J Neurosci*. 2019;39(49):9841-9851. doi:10.1523/JNEUROSCI.1840-19.2019

82. Theriot JJ, Toga AW, Prakash N, Ju YS, Brennan KC. Cortical sensory plasticity in a model of migraine with aura. *J Neurosci*. 2012;32(44):15252-15261. doi:10.1523/JNEUROSCI.2092-12.2012

83. Haider B, McCormick DA. Rapid neocortical dynamics: cellular and network mechanisms. *Neuron*. 2009;62(2):171-189. doi:10.1016/j.neuron.2009.04.008

84. Petersen CCH, Hahn TTG, Mehta M, Grinvald A, Sakmann B. Interaction of sensory responses with spontaneous depolarization in layer 2/3 barrel cortex. *PNAS*. 2003;100(23):13638-13643. doi:10.1073/pnas.2235811100

85. Zagha E, McCormick DA. Neural control of brain state. *Curr Opin Neurobiol*. 2014;29:178-186. doi:10.1016/j.conb.2014.09.010

86. Bragin A, Benassi SK, Engel J. Patterns of the Up-Down State in normal and epileptic mice. *Neuroscience*. 2012;225:76-87. doi:10.1016/j.neuroscience.2012.08.059

87. Gerkin RC, Clem RL, Shruti S, Kass RE, Barth AL. Cortical Up State Activity Is Enhanced After Seizures: A Quantitative Analysis. *J Clin Neurophysiol*. 2010;27(6):425-432. doi:10.1097/WNP.0b013e3181fdf8bd

88. Hodkinson DJ, Wilcox SL, Veggeberg R, et al. Increased Amplitude of Thalamocortical Low-Frequency Oscillations in Patients with Migraine. *J Neurosci*. 2016;36(30):8026-8036. doi:10.1523/JNEUROSCI.1038-16.2016

89. Thanawala MS, Regehr WG. Presynaptic calcium influx controls neurotransmitter release in part by regulating the effective size of the readily releasable pool. *J Neurosci*. 2013;33(11):4625-4633. doi:10.1523/JNEUROSCI.4031-12.2013

90. Ruiz R, Cano R, Casañas JJ, Gaffield MA, Betz WJ, Tabares L. Active Zones and the Readily Releasable Pool of Synaptic Vesicles at the Neuromuscular Junction of the Mouse. *J Neurosci*. 2011;31(6):2000-2008. doi:10.1523/JNEUROSCI.4663-10.2011

91. Murthy VN, Schikorski T, Stevens CF, Zhu Y. Inactivity Produces Increases in Neurotransmitter Release and Synapse Size. *Neuron*. 2001;32(4):673-682. doi:10.1016/S0896-6273(01)00500-1

92. Rizzoli SO, Betz WJ. Synaptic vesicle pools. *Nature Reviews Neuroscience*. 2005;6(1):57-69. doi:10.1038/nrn1583

93. Cesca F, Baldelli P, Valtorta F, Benfenati F. The synapsins: key actors of synapse function and plasticity. *Prog Neurobiol*. 2010;91(4):313-348. doi:10.1016/j.pneurobio.2010.04.006

94. Fiumara F, Milanese C, Corradi A, et al. Phosphorylation of synapsin domain A is required for post-tetanic potentiation. *J Cell Sci*. 2007;120(Pt 18):3228-3237. doi:10.1242/jcs.012005

95. Rodríguez-Castañeda F, Maestre-Martínez M, Coudevylle N, et al. Modular architecture of Munc13/calmodulin complexes: dual regulation by Ca2+ and possible function in short-term synaptic plasticity. *EMBO J.* 2010;29(3):680-691. doi:10.1038/emboj.2009.373

96. Deng L, Kaeser PS, Xu W, Südhof TC. RIM proteins activate vesicle priming by reversing autoinhibitory homodimerization of Munc13. *Neuron*. 2011;69(2):317-331. doi:10.1016/j.neuron.2011.01.005

97. Andrews-Zwilling YS, Kawabe H, Reim K, Varoqueaux F, Brose N. Binding to Rab3A-interacting molecule RIM regulates the presynaptic recruitment of Munc13-1 and ubMunc13-2. *J Biol Chem*. 2006;281(28):19720-19731. doi:10.1074/jbc.M601421200

98. Pyle RA, Schivell AE, Hidaka H, Bajjalieh SM. Phosphorylation of synaptic vesicle protein 2 modulates binding to synaptotagmin. *J Biol Chem*. 2000;275(22):17195-17200. doi:10.1074/jbc.M000674200

99. LaBella ML, Hujber EJ, Moore KA, et al. Casein Kinase 1δ Stabilizes Mature Axons by Inhibiting Transcription Termination of Ankyrin. *Developmental Cell*. 2020;52(1):88-103.e18. doi:10.1016/j.devcel.2019.12.005

100. Mozhayeva MG, Sara Y, Liu X, Kavalali ET. Development of Vesicle Pools during Maturation of Hippocampal Synapses. *J Neurosci*. 2002;22(3):654-665. doi:10.1523/JNEUROSCI.22-03-00654.2002

101. Bornschein G, Brachtendorf S, Schmidt H. Developmental Increase of Neocortical Presynaptic Efficacy via Maturation of Vesicle Replenishment. *Front Synaptic Neurosci*. 2020;11. doi:10.3389/fnsyn.2019.00036

102. Meis S, Endres T, Munsch T, Lessmann V. Presynaptic Regulation of Tonic Inhibition by Neuromodulatory Transmitters in the Basal Amygdala. *Mol Neurobiol*. 2018;55(11):8509-8521. doi:10.1007/s12035-018-0984-1

103. Song I, Volynski K, Brenner T, Ushkaryov Y, Walker M, Semyanov A. Different transporter systems regulate extracellular GABA from vesicular and non-vesicular sources. *Front Cell Neurosci*. 2013;7. doi:10.3389/fncel.2013.00023

104. Richerson GB, Wu Y. Dynamic equilibrium of neurotransmitter transporters: not just for reuptake anymore. *J Neurophysiol*. 2003;90(3):1363-1374. doi:10.1152/jn.00317.2003

105. Wu Y, Wang W, Richerson GB. GABA transaminase inhibition induces spontaneous and enhances depolarization-evoked GABA efflux via reversal of the GABA transporter. *J Neurosci*. 2001;21(8):2630-2639.

106. Wu Y, Wang W, Díez-Sampedro A, Richerson GB. Nonvesicular inhibitory neurotransmission via reversal of the GABA transporter GAT-1. *Neuron*. 2007;56(5):851-865. doi:10.1016/j.neuron.2007.10.021

107. Medrihan L, Ferrea E, Greco B, Baldelli P, Benfenati F. Asynchronous GABA Release Is a Key Determinant of Tonic Inhibition and Controls Neuronal Excitability: A Study in the Synapsin II-/- Mouse. *Cereb Cortex*. 2015;25(10):3356-3368. doi:10.1093/cercor/bhu141

108. Gulledge AT, Stuart GJ. Excitatory Actions of GABA in the Cortex. *Neuron*. 2003;37(2):299-309. doi:10.1016/S0896-6273(02)01146-7

109. Staley KJ, Mody I. Shunting of excitatory input to dentate gyrus granule cells by a depolarizing GABAA receptor-mediated postsynaptic conductance. *Journal of Neurophysiology*. 1992;68(1):197-212. doi:10.1152/jn.1992.68.1.197

110. Pathak HR, Weissinger F, Terunuma M, et al. Disrupted Dentate Granule Cell Chloride Regulation Enhances Synaptic Excitability during Development of Temporal Lobe Epilepsy. *J Neurosci*. 2007;27(51):14012-14022. doi:10.1523/JNEUROSCI.4390-07.2007

111. Scimemi A. Structure, function, and plasticity of GABA transporters. *Front Cell Neurosci*. 2014;8. doi:10.3389/fncel.2014.00161

Figure legends

Figure 1. Increased up state duration and V_m variance found in CK1δ$_{T44A}$ mice, despite hyperpolarized neuronal resting V_m. (**A**) Schematic of *in vivo* whole-cell patch-clamp experiment along with representative current-clamp traces (L2/3 pyramidal neurons) of up and down states from WT and CK1δ$_{T44A}$ mice. (**B**) CK1δ$_{T44A}$ neurons were significantly hyperpolarized compared to WT. (**C**) Frequency histograms of upstate half-width show a positive shift in the upstate durations in CK1δ$_{T44A}$ mice. (**D**) CK1δ$_{T44A}$ mice show an increase in the mean up-state durations of individual animals and (**E**) an increase in membrane potential variance (standard deviation) during up states. Statistical analyses: unpaired t-test (B and D), 2-sample KS test (C and E,). Pooled data are means ± SD. *P < 0.05, **P < 0.01, and ****P < 0.0001. Exact P values can be found in table S1.

Figure 2. Increased tonic inhibition in CK1δ$_{T44A}$ neurons primarily contributes to hyperpolarized resting V_m. (**A**) Schematic showing *in vitro* whole-cell patch-clamp electrophysiology in acute coronal brain slices and a representative image of a typical biocytin-labeled excitatory L2/3 neuron. (**B**) Significantly hyperpolarized resting membrane potentials in CK1δ$_{T44A}$ neurons compared to WT. (**C**) Representative trace from a WT neuron showing a reduction in tonic inhibitory current, after application of 20μM picrotoxin ($GABA_A$ antagonist). Right: % distribution histograms along with gaussian fits (10^4 datapoints) showing PTX sensitive holing current (tonic inhibitory current) as the difference between the % distribution

means. (**D**) Tonic inhibitory currents were significantly larger in CK1δ_{T44A} neurons compared to WT. (**E**) Representative traces from a WT neuron showing resting membrane potential as well as voltage response to depolarizing current pulse before and after picrotoxin application. (**F**) The difference in the resting membrane potential between individual WT neurons as well as CK1δ_{T44A} neurons before and after picrotoxin treatment. (**G**) Pharmacological blockade of tonic inhibitory current lead to the 'rescue' of hyperpolarized membrane potentials in CK1δ_{T44A}neurons. Statistical analyses: unpaired t-test (B), Mann Whitney test (D), paired t-test (F), and two-way ANOVA (G). Pooled data are means ± SEM. *P < 0.05, **P < 0.01, and ***P < 0.001. Exact P values can be found in table S1.

Figure 3. Increased evoked action potential frequency in CK1δ_{T44A} neurons was due to increased synaptic feedback excitation. (**A**) Representative traces of L2/3 excitatory neurons firing action potentials to suprathreshold current injections. (**B**) AP frequency in CK1δ_{T44A} neurons was significantly increased, especially at higher input currents along with the slopes of linear regression lines fitted to the FI plots. (**C**) Comparison of FI slopes quantified for individual neurons revealed that CK1δT44A had significantly higher FI slopes compared to WT. (**D**) No significant difference in rheobase between WT and CK1δT44A neurons. (**E**) Representative AP traces for WT and CK1δ_{T44A} neurons, as well as phase plots showing the rate of change of V_m during APs as a function of V_m (dV_m/dt vs V_m). (**F**) No difference was observed in AP half-width as well as (**G**) the after-hyperpolarization (AHP) amplitude. (**H**) Representative traces of WT and CK1δ_{T44A} neurons firing action potentials in response to 400pA current injection. (**I**) Comparison of inter-spike interval between WT and CK1δ_{T44A} neurons was significantly reduced following 400pA current injection, suggesting reduced spike frequency adaptation. (**J**) However, the inter-spike interval was not different in CK1δ_{T44A} neurons at 300pA. (**K**) Schematic showing pharmacological inhibition of postsynaptic glutamate receptors to block synaptic excitation during intracellular current injections. (**L**) Action potential frequency/input current (F/I) plots demonstrating that inhibition of postsynaptic glutamate receptors normalized the input-current-dependent increase in AP frequency seen in CK1δ_{T44A} neurons to WT levels. (**M**) No difference in the slopes of the linear regression fitted to the FI plots for individual neurons, between genotypes. Statistical analyses: Two-way ANOVA with Dunnett's test for multiple comparisons (B, I and J), unpaired t-test (C, F, G, and M), ANCOVA (B), and Mann Whitney test (D). Pooled data are means ± SEM. *P < 0.05 and **P < 0.01. Exact P values can be found in table S1.

Figure 4. Stimulus-frequency-dependent adaptation deficits due to increased RRP size at CK1δ_{T44A} excitatory synapses. (**A**) Schematic representation of L2/3 cortical microcircuit showing the placement of stimulation as well as recording electrodes. (**B**) Representative traces showing evoked EPSC and IPSC responses to a train of 30 stimuli, at 20Hz. Traces of EPSCs evoked to the first two stimuli (**B'**), used for the quantification of paired-pulse ratio (PPR). (**C**) No significant difference between genotypes in the normalized EPSC amplitude as well as PPR at 10Hz and (**D**) 20Hz stimulus trains. (**E**) Normalized evoked EPSC response to 50Hz stimulus train was significantly higher at CK1δ_{T44A} synapse. *Inset:* significant difference in the paired-pulse ratio (PPR) at 50Hz between genotypes. (**F**) Schematic of a model synapse showing dynamic regulation of readily releasable pool (RRP) with simultaneous release and replenishment of synaptic vesicles upon repeated stimulation. (**G**) Schematic showing the analytical approach employed to explore the components of the presynaptic release machinery (RRP size and replenishment rate). (**H to J**) Cumulative amplitude plot for mean EPSC amplitudes: There was no significant difference in the slope of the linear regression fitted to the steady state between WT and CK1δT44A at any stimulus frequency. However, y-intercepts of the linear regression were significantly different between genotypes at both 20Hz (**I**) and 50Hz (**J**). (**K to M**) Slopes and y-intercepts for individual neurons: No significant difference in slopes, but significant difference in y-intercept at 50Hz (**M**). Statistical analyses: Repeated measures Two-way ANOVA with Dunnett's test for multiple comparisons and unpaired t-test (C, D, and E), ANCOVA (H, I, and J), unpaired t-test or Mann Whitney u test (K, L, and M). Pooled data are means ± SEM. *P < 0.05 and ****P < 0.0001. Exact P values in table S1.

Figure 5. Impaired adaptation of evoked EPSCs at high stimulation frequencies was dependent on $[Ca^{2+}]_e$. (**A**) Schematic showing cortical microcircuits and experimental design to record evoked EPSCs in presence of low $[Ca^{2+}]_e$. (**B**) Representative race showing evoked EPSCs (at 10, 20, and 50Hz) recorded in low Ca^{2+} (0.65mM) ACSF, in response to a train of 30 stimuli. (**C to E**) In low $[Ca^{2+}]_e$ conditions, we found no difference in normalized EPSC amplitude and PPR between WT and CK1δ_{T44A} neurons at any frequency. (**F to H**) Similarly, we found no difference in the y-intercepts of linear regressions fitted to the steady-state cumulative EPSCs, in low $[Ca^{2+}]_e$ conditions between WT and CK1δ_{T44A} neurons. (**I and J**) In low $[Ca^{2+}]_e$ conditions, linear regression y-intercepts and the slopes of the cumulative EPSCs quantified for individual neurons were not different between genotypes for any stimulation frequency. Statistical analyses: repeated measures two-way ANOVA (C, D, and E), ANCOVA

(F, G, and H), and unpaired t-test (C, D, E, I, and J). Pooled data are means ± SEM. Exact P values in table S1

Figure 6. Larger glutamate transients in CK1δ$_{T44A}$ slices evoked by high-frequency stimulation. (**A**) Schematic showing experimental design for two-photon fluorescent glutamate imaging in acute slices with a representative image of a limited area scan (100 lines/frame at 79.80 Hz) showing viral expression of iGluSnFR in neurons, (left). Image panels showing stimulus-evoked glutamate transient response over time, (50 Hz train of 30 stimuli, scale: 200µm, **Movie S2**). (**B**) Representative traces of evoked glutamate transient responses at 10, 20, and 50 Hz, in WT and CK1δ$_{T44A}$ slices. (**C**) Traces of glutamate transient responses for individual slices (gray) and grand means (WT: cyan, CK1δ$_{T44A}$: purple) evoked after 10Hz stimulation. (**D**) At 10Hz, the amplitude and area under the curve (AUC) of evoked glutamate transients were not significantly higher in CK1δ$_{T44A}$ slices. (**E**) Traces of glutamate transient responses for individual slices and grand means evoked after 20Hz stimulation. (**F**) No difference in the amplitude or AUC of evoked glutamate transients evoked to 20Hz stimuli. (**G**) Traces of glutamate transient responses for individual slices and grand means evoked after 50Hz stimulation. (**H**) Both amplitude and AUC of glutamate transients evoked to 50Hz stimuli were significantly increased in CK1δ$_{T44A}$ slices. Statistical analyses: Mann Whitney test (F and H) and unpaired t-test (D). Pooled data are means ± SEM. **P < 0.01. Exact P values in table S1.

Figure 7. An excitatory shift in the cortical circuits found in CK1δ$_{T44A}$ mice. (**A**) Schematic showing cortical microcircuit and experimental design along with representative traces of evoked E/IPSCs from a WT neuron in response to a train of 10 stimuli, recorded from the same neuron. (**B to D**) At 50Hz (**D**), E/IPSC amplitude ratios (E/I ratio) recorded from individual neurons show a significant shift towards excitation in CK1δ$_{T44A}$ neurons. No difference in the E/I ratio between genotypes at 20Hz and 10Hz (**B** and **C**). (**E**) Representative traces showing inhibitory (V_{clamp} +20mV) and excitatory (V_{clamp} -70mV) synaptic barrages recorded in voltage clamp mode during an upstate *in vivo* (**F**) Comparison of IPSC half-width (animal means, left) shows no difference between WT and CK1δ$_{T44A}$ mice. Frequency histograms of % distributions (right) show only a modest shift in half-width of the inhibitory events in CK1δ$_{T44A}$ mice. (**G**) Comparison of EPSC half-width (animal means, left) shows a significant increase in CK1δ$_{T44A}$ mice along with a frequency histogram of % distributions (right) showing a positive shift in half-width distribution of the excitatory events in CK1δ$_{T44A}$ mice. (**H**) Schematic showing

experimental design as well as an example image sequence showing the progression of a focally induced SD wave across space and time under control conditions (scale bar: 200 µm, **Movie S3**). Representative traces showing an increase in transmittance ($\Delta T/T_0$), obtained from an ROI 500µm from the induction site, as well as intracellular voltage rise recorded from different WT slices (arrows indicating the time of SD ignition). (**I**) CK1δ_{T44A} slices exhibit significantly reduced SD thresholds that were partially rescued in low $[Ca^{2+}]_e$ conditions. Statistical analyses: Repeated measures Two-way ANOVA (B, C, and D), Two-way ANOVA with Tukey's test for multiple comparisons (I), Mann Whitney u test, and two-sample KS test (F and G). Pooled data are means ± SEM. *P < 0.05. Exact P values in table S1.

Figure 8. Model of cortical network excitability in CK1δ_{T44A} mice. (A) CK1δ_{T44A} excitatory (not inhibitory) synapses demonstrated reduced presynaptic adaptation to repeated high-frequency stimuli, mediated by a $[Ca^{2+}]_e$-dependent enhancement of RRP size, despite normal synaptic transmission at rest. **(B)** This led to an increase in the glutamate release and a resultant increase in cumulative amplitude of evoked EPSCs along with a higher excitation-to-inhibition ratio during sustained activity, both *in vivo* and in brain slices. **(C)** At the local microcircuit level, trains of action potentials elicited from single neurons increased glutamatergic feedback excitation in CK1δ_{T44A} compared to WT brain slices, further increasing firing frequencies at more intense input currents. **(D)** At a network level, CK1δ_{T44A} mice show an increase in the duration of up state activity *in vivo*, which is dependent on local circuit synaptic feedback excitation. Finally, SD susceptibility in CK1δ_{T44A} brain slices was returned to WT levels with the reduced $[Ca^{2+}]_e$, consistent with presynaptic contributions to the phenotype. Together, these findings show a presynaptic stimulus-dependent glutamatergic gain of function mediates a cortical network-level hyperexcitability phenotype in CK1δ_{T44A} mice.

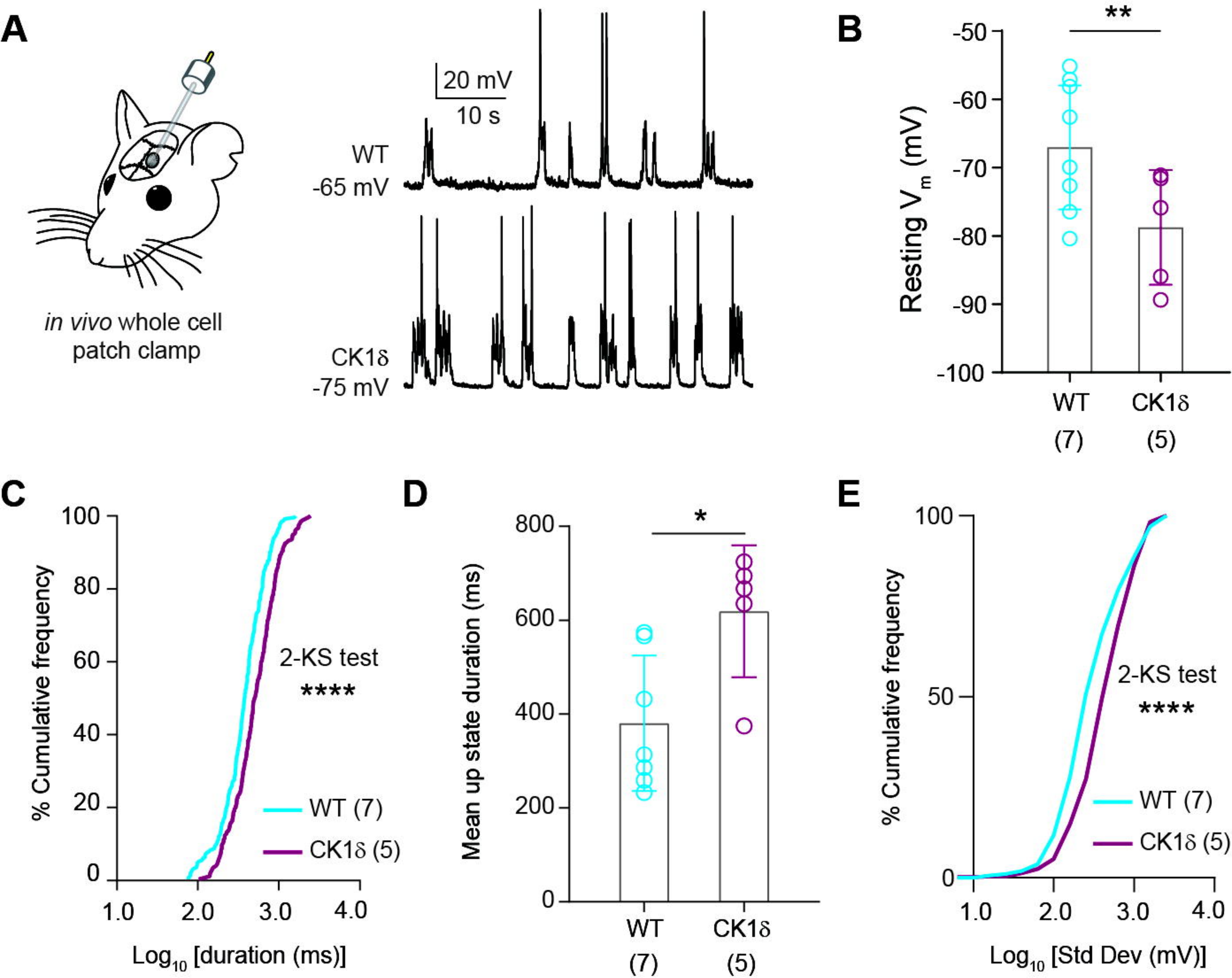
A
in vivo whole cell patch clamp
20 mV
10 s
WT
-65 mV
CK1δ
-75 mV
B
**
Resting V_m (mV)
-50
-60
-70
-80
-90
-100
WT
(7)
CK1δ
(5)
C
% Cumulative frequency
100
80
60
40
20
0
2-KS test
****
WT (7)
CK1δ (5)
1.0
2.0
3.0
4.0
Log_{10} [duration (ms)]
D
*
Mean up state duration (ms)
800
600
400
200
0
WT
(7)
CK1δ
(5)
E
% Cumulative frequency
100
50
0
2-KS test
****
WT (7)
CK1δ (5)
1.0
2.0
3.0
4.0
Log_{10} [Std Dev (mV)]

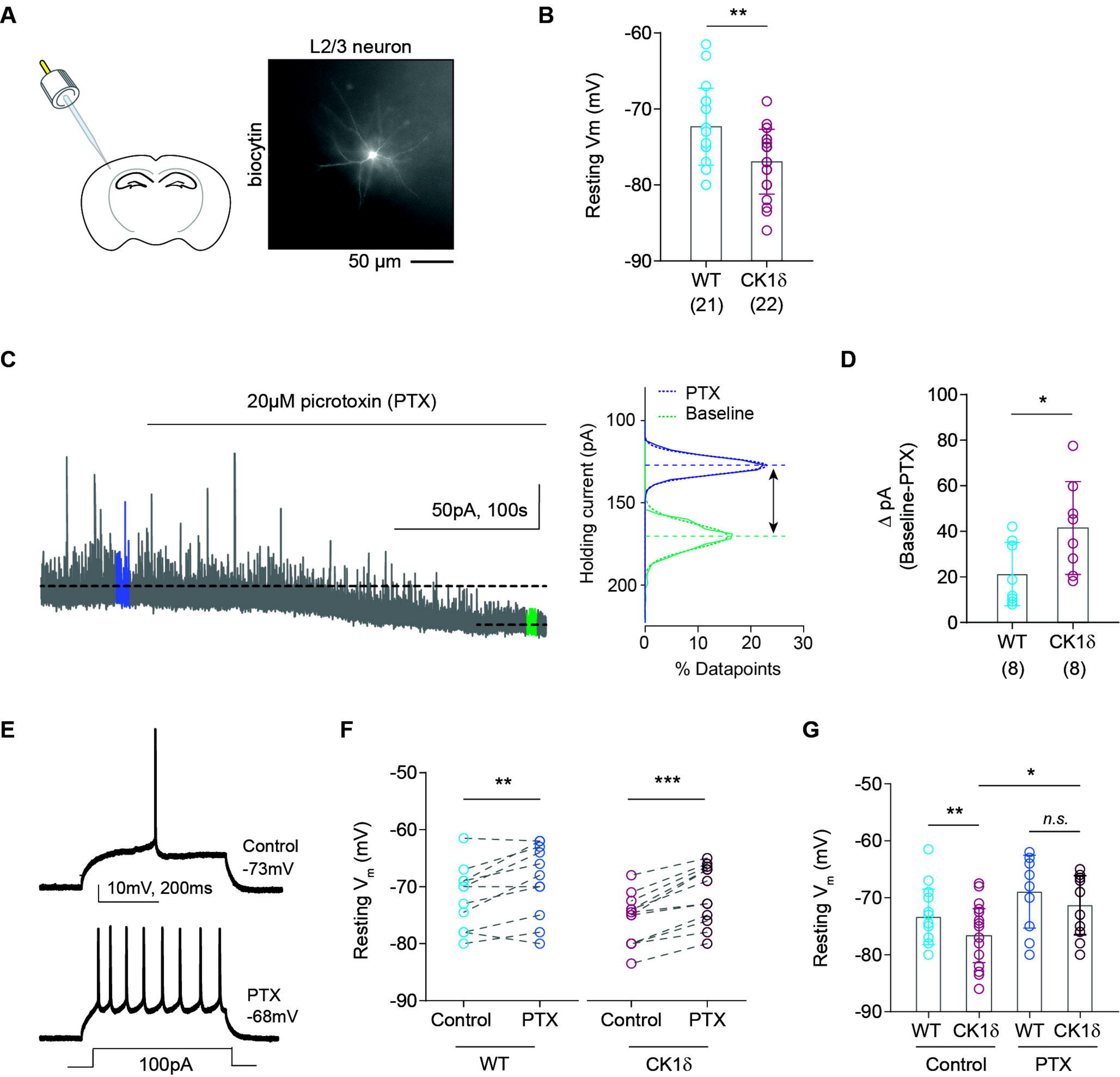
A
L2/3 neuron
biocytin
50 µm
B
**
Resting Vm (mV)
-60
-70
-80
-90
WT
(21)
CK1δ
(22)
C
20µM picrotoxin (PTX)
50pA, 100s
PTX
Baseline
Holding current (pA)
100
150
200
0
10
20
30
% Datapoints
D
*
Δ pA
(Baseline-PTX)
100
80
60
40
20
0
WT
(8)
CK1δ
(8)
E
Control
-73mV
10mV, 200ms
PTX
-68mV
100pA
F
**
***
Resting Vm (mV)
-50
-60
-70
-80
-90
Control
PTX
Control
PTX
WT
CK1δ
G
*
**
n.s.
Resting Vm (mV)
-50
-60
-70
-80
-90
WT
CK1δ
WT
CK1δ
Control
PTX

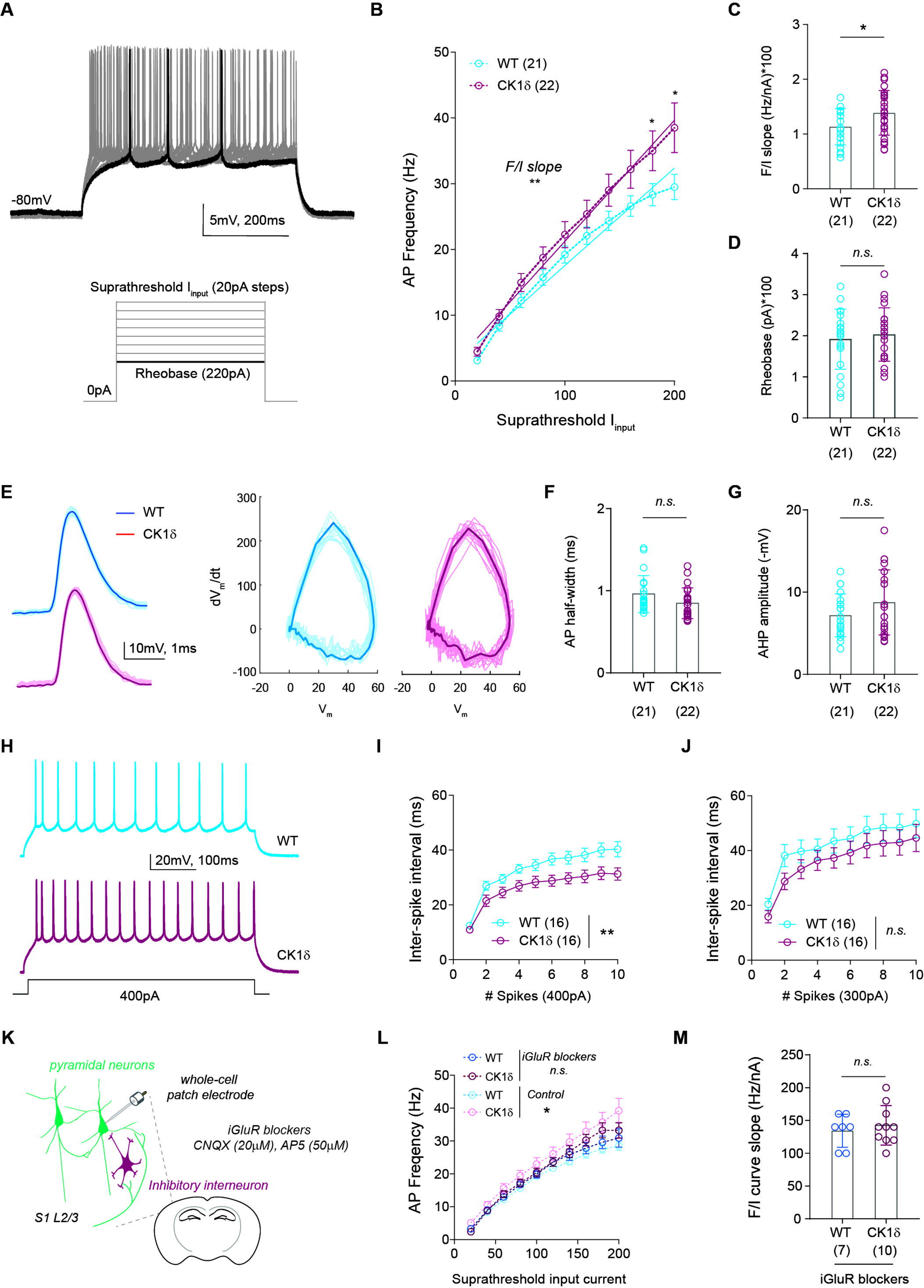
A
-80mV
5mV, 200ms
Suprathreshold I_input (20pA steps)
Rheobase (220pA)
0pA
B
WT (21)
CK1δ (22)
F/I slope
**
AP Frequency (Hz)
Suprathreshold I_input
C
F/I slope (Hz/nA)*100
WT (21)
CK1δ (22)
D
n.s.
Rheobase (pA)*100
E
WT
CK1δ
10mV, 1ms
dV_m/dt
V_m
F
AP half-width (ms)
G
AHP amplitude (-mV)
H
WT
20mV, 100ms
CK1δ
400pA
I
Inter-spike interval (ms)
WT (16)
CK1δ (16)
Spikes (400pA)
J
Spikes (300pA)
K
pyramidal neurons
whole-cell patch electrode
iGluR blockers
CNQX (20μM), AP5 (50μM)
Inhibitory interneuron
S1 L2/3
L
iGluR blockers
Control
AP Freqency (Hz)
Suprathreshold input current
M
F/I curve slope (Hz/nA)
WT (7)
CK1δ (10)
iGluR blockers

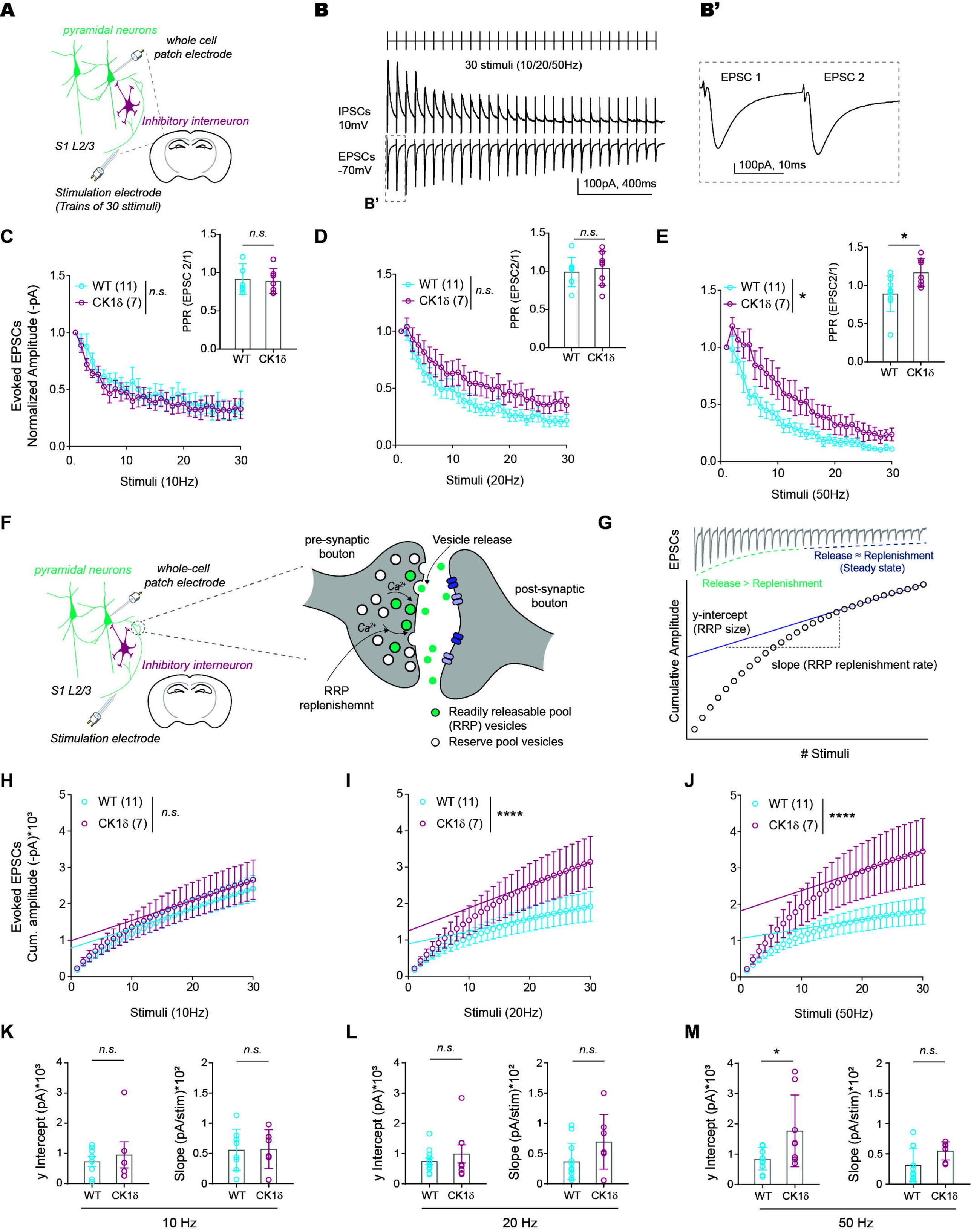
A
pyramidal neurons
whole cell patch electrode
Inhibitory interneuron
S1 L2/3
Stimulation electrode (Trains of 30 sttimuli)
B
30 stimuli (10/20/50Hz)
IPSCs 10mV
EPSCs -70mV
100pA, 400ms
B'
EPSC 1
EPSC 2
100pA, 10ms
C
Evoked EPSCs Normalized Amplitude (-pA)
WT (11)
CK1δ (7)
n.s.
PPR (EPSC 2/1)
Stimuli (10Hz)
D
PPR (EPSC2/1)
Stimuli (20Hz)
E
*
Stimuli (50Hz)
F
pyramidal neurons
whole-cell patch electrode
Inhibitory interneuron
S1 L2/3
Stimulation electrode
pre-synaptic bouton
Vesicle release
post-synaptic bouton
RRP replenishemnt
Readily releasable pool (RRP) vesicles
Reserve pool vesicles
G
EPSCs
Release ≈ Replenishment (Steady state)
Release > Replenishment
Cumulative Amplitude
y-intercept (RRP size)
slope (RRP replenishment rate)
Stimuli
H
Evoked EPSCs Cum. amplitude (-pA)*10³
I
****
J
K
y Intercept (pA)*10³
Slope (pA/stim)*10²
WT
CK1δ
10 Hz
L
20 Hz
M
50 Hz

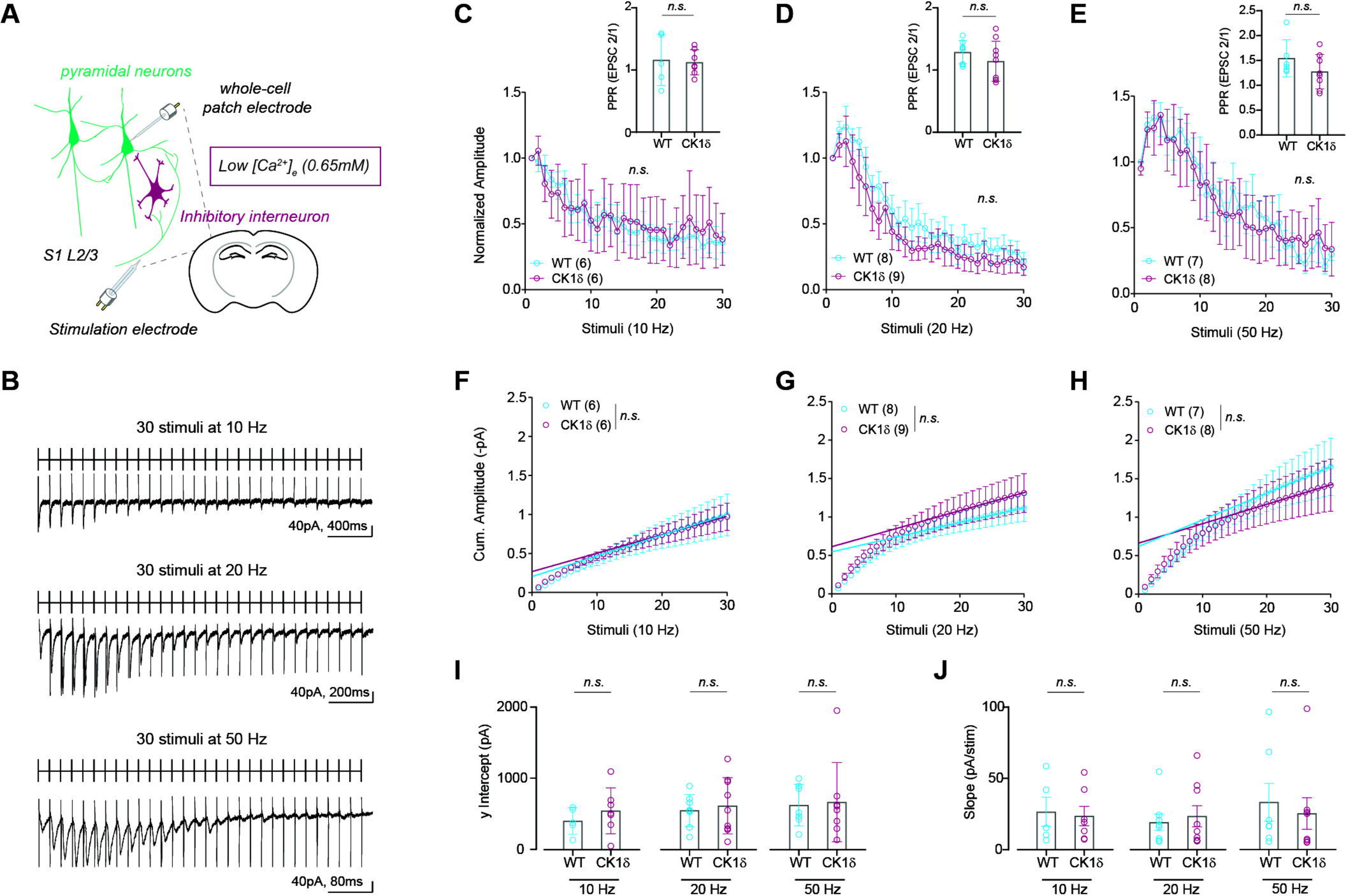
A
pyramidal neurons
whole-cell patch electrode
Low [Ca2+]e (0.65mM)
Inhibitory interneuron
S1 L2/3
Stimulation electrode
B
30 stimuli at 10 Hz
40pA, 400ms
30 stimuli at 20 Hz
40pA, 200ms
30 stimuli at 50 Hz
40pA, 80ms
C
D
E
PPR (EPSC 2/1)
n.s.
WT
CK1δ
Normalized Amplitude
WT (6)
CK1δ (6)
WT (8)
CK1δ (9)
WT (7)
CK1δ (8)
Stimuli (10 Hz)
Stimuli (20 Hz)
Stimuli (50 Hz)
F
G
H
Cum. Amplitude (-pA)
I
J
y Intercept (pA)
Slope (pA/stim)
10 Hz
20 Hz
50 Hz

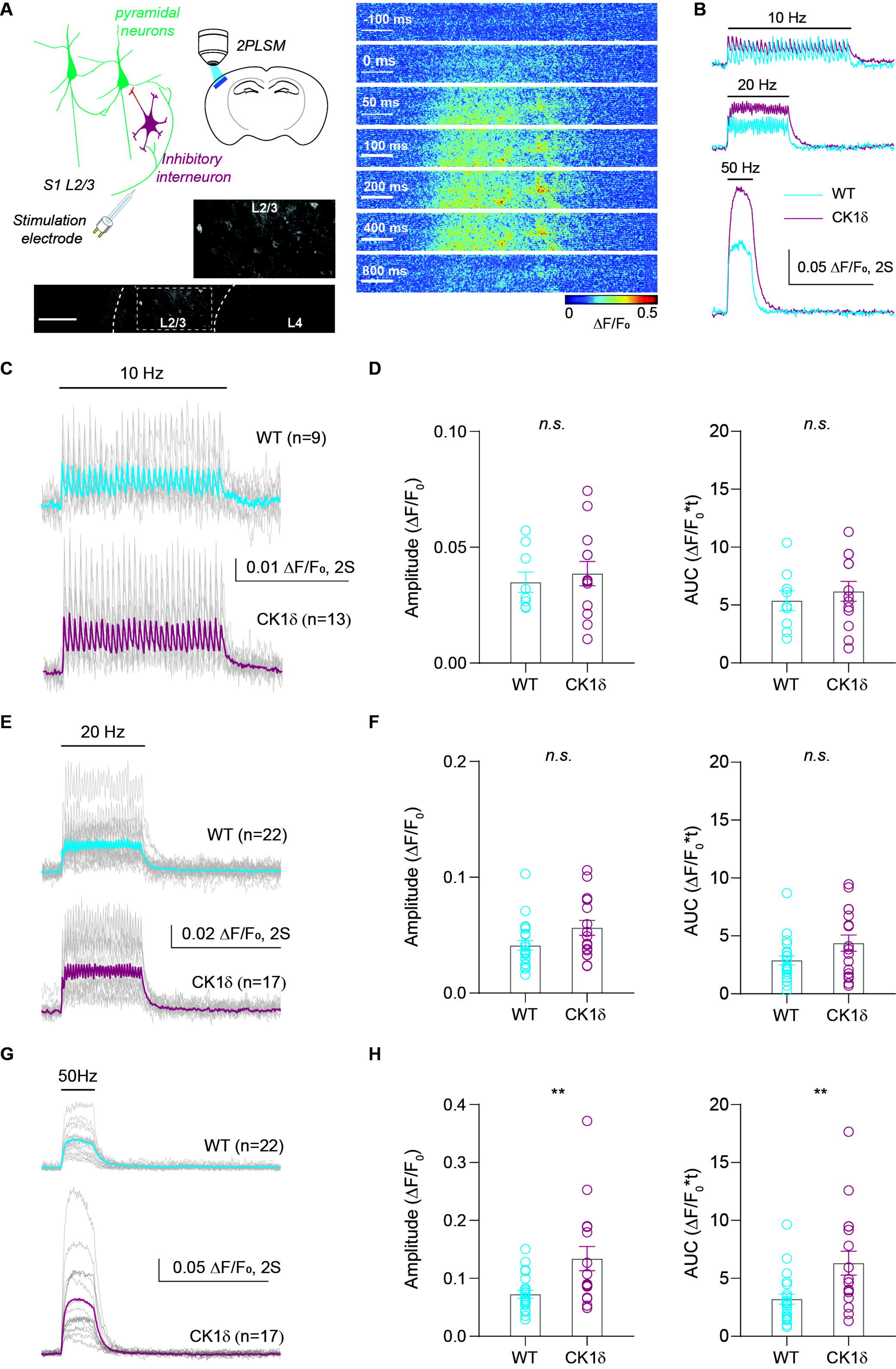
A
pyramidal neurons
2PLSM
Inhibitory interneuron
S1 L2/3
Stimulation electrode
L2/3
L2/3
L4
-100 ms
0 ms
50 ms
100 ms
200 ms
400 ms
800 ms
0
0.5
ΔF/F₀
B
10 Hz
20 Hz
50 Hz
WT
CK1δ
0.05 ΔF/F₀, 2S
C
10 Hz
WT (n=9)
0.01 ΔF/F₀, 2S
CK1δ (n=13)
D
n.s.
Amplitude (ΔF/F0)
AUC (ΔF/F0*t)
WT
CK1δ
E
20 Hz
WT (n=22)
0.02 ΔF/F₀, 2S
CK1δ (n=17)
F
n.s.
G
50Hz
WT (n=22)
0.05 ΔF/F₀, 2S
CK1δ (n=17)
H
**

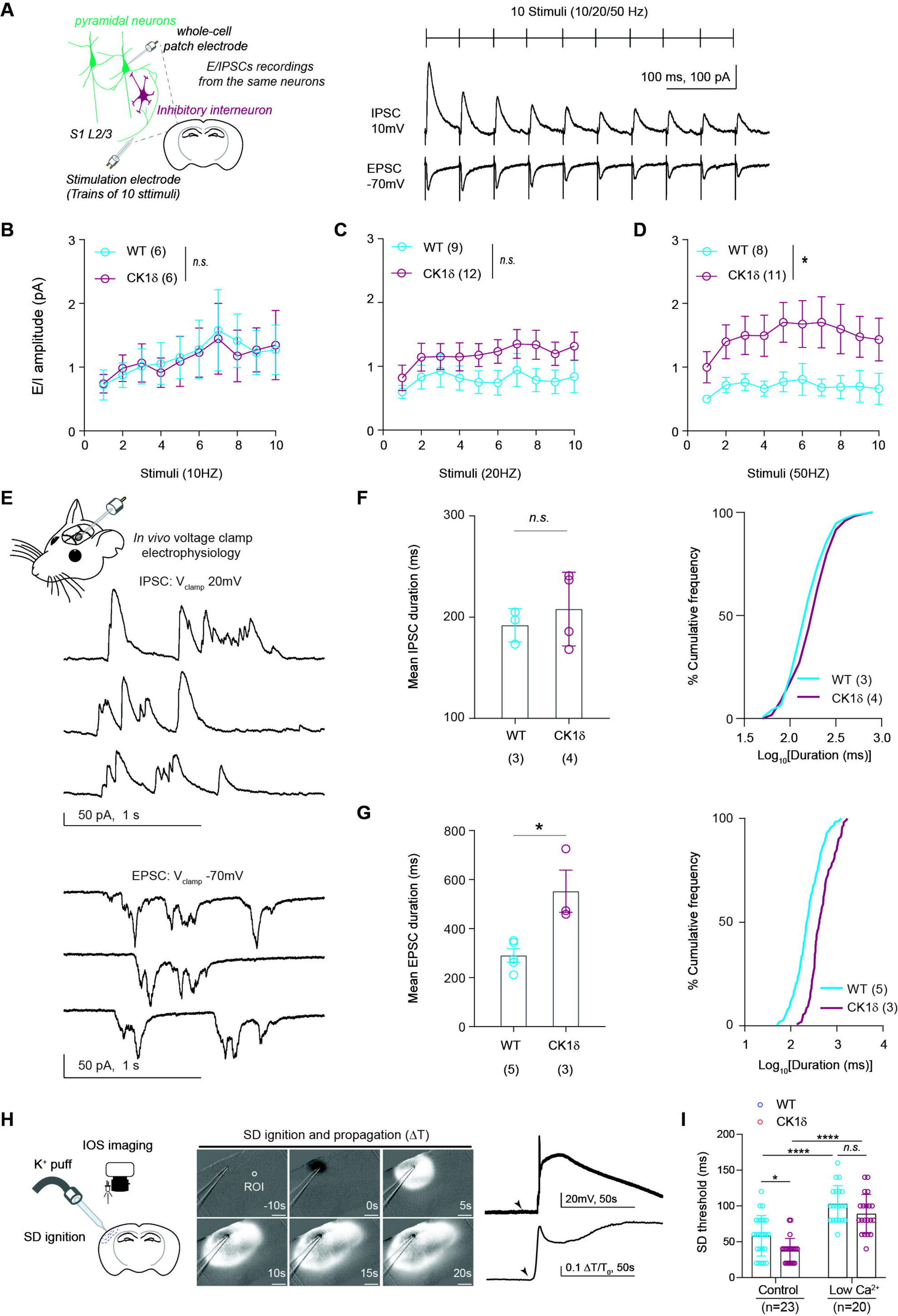
A
pyramidal neurons
whole-cell patch electrode
E/IPSCs recordings from the same neurons
Inhibitory interneuron
S1 L2/3
Stimulation electrode (Trains of 10 sttimuli)
10 Stimuli (10/20/50 Hz)
100 ms, 100 pA
IPSC 10mV
EPSC -70mV
B
WT (6)
CK1δ (6)
n.s.
E/I amplitude (pA)
Stimuli (10HZ)
C
WT (9)
CK1δ (12)
n.s.
Stimuli (20HZ)
D
WT (8)
CK1δ (11)
*
Stimuli (50HZ)
E
In vivo voltage clamp electrophysiology
IPSC: V clamp 20mV
50 pA, 1 s
EPSC: V clamp -70mV
50 pA, 1 s
F
n.s.
Mean IPSC duration (ms)
WT (3)
CK1δ (4)
% Cumulative frequency
Log10[Duration (ms)]
G
*
Mean EPSC duration (ms)
WT (5)
CK1δ (3)
% Cumulative frequency
Log10[Duration (ms)]
H
IOS imaging
K+ puff
SD ignition
SD ignition and propagation (ΔT)
ROI
-10s
0s
5s
10s
15s
20s
20mV, 50s
0.1 ΔT/T0, 50s
I
WT
CK1δ
SD threshold (ms)
Control (n=23)
Low Ca2+ (n=20)
n.s.
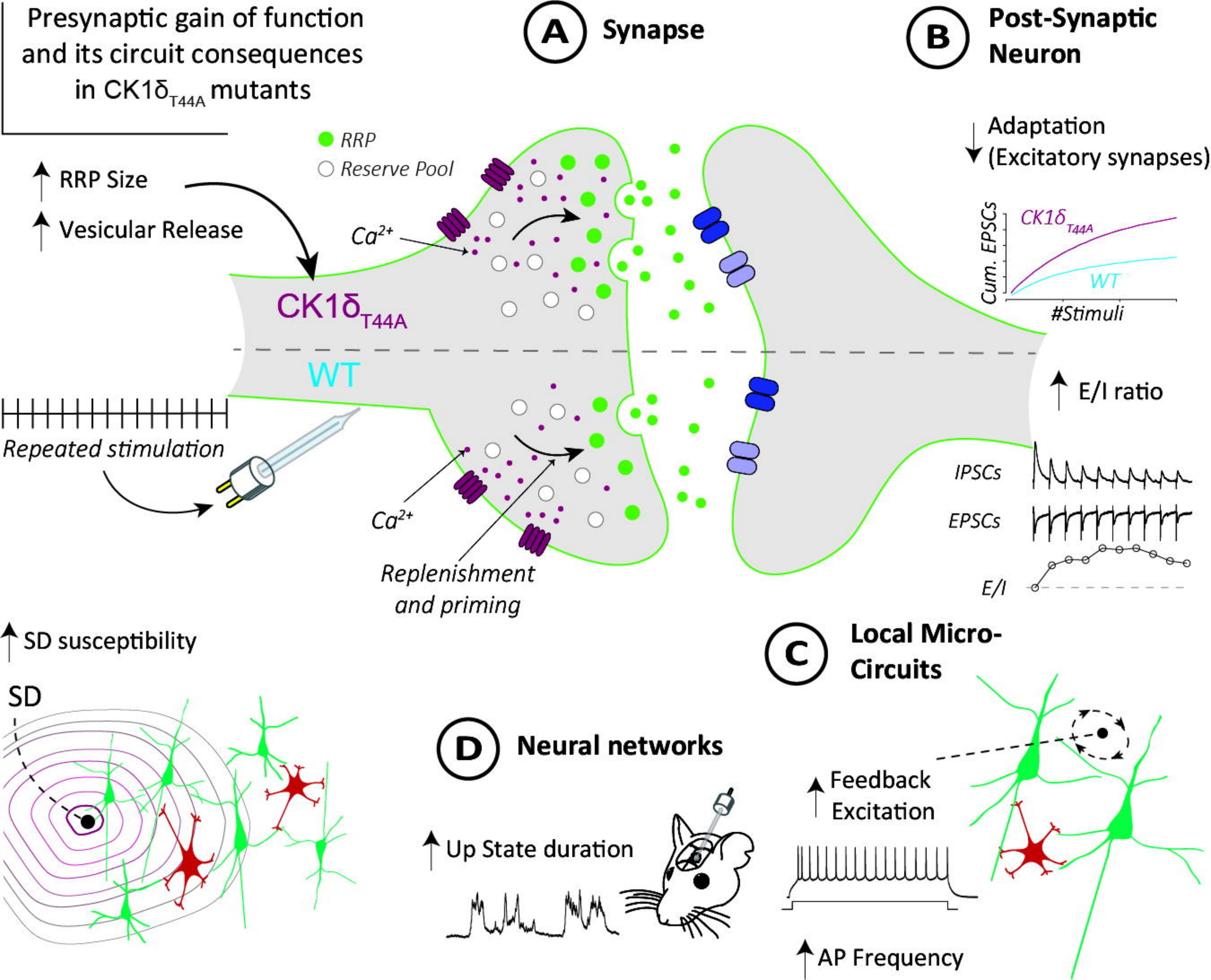
Presynaptic gain of function and its circuit consequences in CK1δ$_{T44A}$ mutants